Cell Reports
Medicine

Article

Targeting of vulnerabilities of drug-tolerant persisters identified through functional genetics delays tumor relapse

Graphical abstract

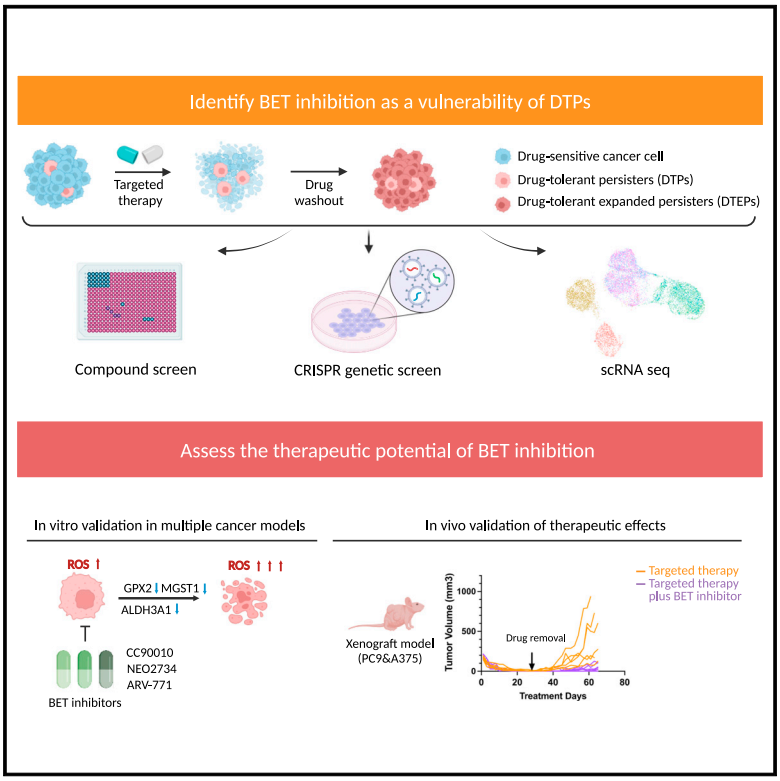

Highlights

- Unbiased genetic screen and compound screen identify BRD2 as a vulnerability of DTPs
- BET inhibitors suppress outgrowth of DTPs in a broad spectrum of cancer types
- BET inhibitors suppress DTEPs through transcriptional repression of GPX2/ALDH3A1/MGST1
- BET inhibitors delay tumor relapse

Authors

Mengnuo Chen, Sara Mainardi, Cor Lieftink, ..., Roderick L. Beijersbergen, Liqin Wang, René Bernards

Correspondence

l.wang@nki.nl (L.W.), r.bernards@nki.nl (R.B.)

In brief

Chen et al. uses high-throughput screening approaches to identify BRD2 inhibition as a vulnerability of drug-tolerant persisters (DTPs). They further demonstrate that BET inhibitors suppress the emergence of DTPs in multiple cancer cell lines *in vitro* and can forestall drug resistance through the eradication of DTPs *in vivo*.

Chen et al., 2024, Cell Reports Medicine *5*, 101471
March 19, 2024
https://doi.org/10.1016/j.xcrm.2024.101471

CellPress

Cell Reports Medicine

CellPress
OPEN ACCESS

Article

Targeting of vulnerabilities of drug-tolerant persisters identified through functional genetics delays tumor relapse

Mengnuo Chen,[1,4] Sara Mainardi,[1] Cor Lieftink,[1,2] Arno Velds,[3] Iris de Rink,[3] Chen Yang,[4] Hendrik J. Kuiken,[1,2] Ben Morris,[1,2] Finn Edwards,[1] Fleur Jochems,[1] Olaf van Tellingen,[5] Manon Boeije,[6] Natalie Proost,[6] Robin A. Jansen,[1] Shifan Qin,[1] Haojie Jin,[1,4] J.C. Koen van der Mijn,[1,7] Arnout Schepers,[1] Subramanian Venkatesan,[1] Wenxin Qin,[4] Roderick L. Beijersbergen,[1,2,3] Liqin Wang,[1,8,*] and René Bernards[1,9,*]

[1]Division of Molecular Carcinogenesis, Oncode Institute, The Netherlands Cancer Institute, Amsterdam, the Netherlands
[2]NKI Robotics and Screening Center, The Netherlands Cancer Institute, Amsterdam, the Netherlands
[3]Genomics Core Facility, The Netherlands Cancer Institute, Amsterdam, the Netherlands
[4]State Key Laboratory of Oncogenes and Related Genes, Shanghai Cancer Institute, Renji Hospital, Shanghai Jiao Tong University School of Medicine, Shanghai, China
[5]Division of Pharmacology, The Netherlands Cancer Institute, Amsterdam, the Netherlands
[6]Mouse Clinic for Cancer and Aging Research, Preclinical Intervention Unit, The Netherlands Cancer Institute, 1066CX Amsterdam, the Netherlands
[7]Department of Medical Oncology, The Netherlands Cancer Institute, Amsterdam, the Netherlands
[8]State Key Laboratory of Oncology in South China, Sun Yat-sen University Cancer Center, Guangzhou, China
[9]Lead contact
*Correspondence: l.wang@nki.nl (L.W.), r.bernards@nki.nl (R.B.)
https://doi.org/10.1016/j.xcrm.2024.101471

SUMMARY

Drug-tolerant persisters (DTPs) are a rare subpopulation of cells within a tumor that can survive therapy through nongenetic adaptive mechanisms to develop relapse and repopulate the tumor following drug withdrawal. Using a cancer cell line with an engineered suicide switch to kill proliferating cells, we perform both genetic screens and compound screens to identify the inhibition of bromodomain and extraterminal domain (BET) proteins as a selective vulnerability of DTPs. BET inhibitors are especially detrimental to DTPs that have reentered the cell cycle (DTEPs) in a broad spectrum of cancer types. Mechanistically, BET inhibition induces lethal levels of ROS through the suppression of redox-regulating genes highly expressed in DTPs, including GPX2, ALDH3A1, and MGST1. *In vivo* BET inhibitor treatment delays tumor relapse in both melanoma and lung cancer. Our study suggests that combining standard of care therapy with BET inhibitors to eliminate residual persister cells is a promising therapeutic strategy.

INTRODUCTION

Drug-tolerant persisters (DTPs) were initially discovered in subpopulations of bacteria that are resistant to antibiotics through non-inheritable mechanisms associated with proliferation pause.[1,2] In 2010, the existence of similar rare subpopulations of DTPs were identified in non-small cell lung cancer cell lines that survived lethal dosage of targeted/chemotherapy by entering a noncycling state.[3] Slowly cycling DTPs were subsequently identified as having a distinct transcriptomic profile.[4] Different from genetic resistance, the drug-tolerant state is reversible as drug-tolerant expanded persisters (DTEPs) gradually regain proliferative capacity after drug withdrawal and regain sensitivity to primary treatment.[5] DTPs are thought to serve as a reservoir from which genetic resistant variants can emerge.[2,6] Therefore, a better understanding of the selective vulnerabilities of DTPs/DTEPs could enable the development of novel therapeutic strategies.

Since their original discovery in lung cancer, the presence of DTPs has been confirmed in multiple cancer types, including breast cancer, prostate cancer, melanoma, gastric carcinoma, and colon cancer.[1,6] Diverse mechanisms have been reported to promote the formation of DTPs. A number of studies support that epigenetic reprogramming, which involves altered histone modifications and promoter region accessibilities, promotes cancer cells to enter this non-genetic and reversible DTP status.[2,3,5] In addition, YAP-mediated enhanced expression of anti-apoptotic signaling has been shown to empower DTPs to evade drug-induced apoptosis.[7] Also, adaptive activation of inflammatory signaling, including nuclear factor κB (NF-κB), interferon response, and signal transducer and activator of transcription 3 (STAT3) have also been reported to play a role in hampering drug-induced death.[8,9] Moreover, DTPs also have features of epithelial-mesenchymal transition (EMT), which is known to be associated with poor drug responsiveness, a senescence-like gene signature, altered metabolic and proteomic

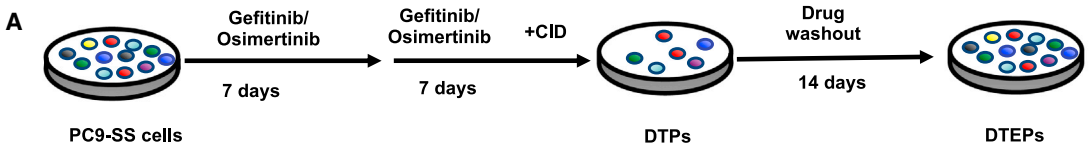

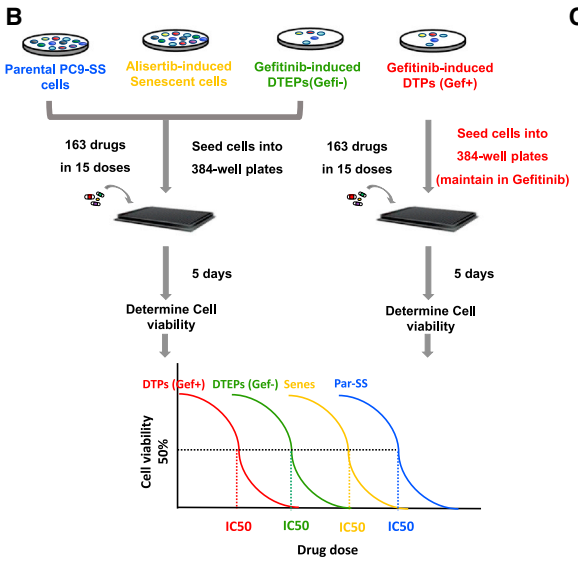

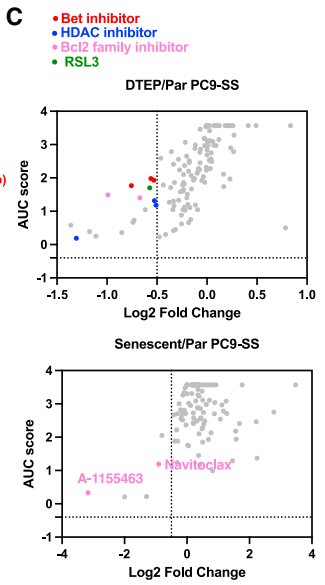

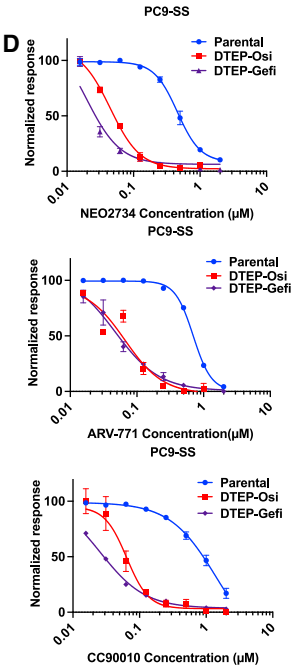

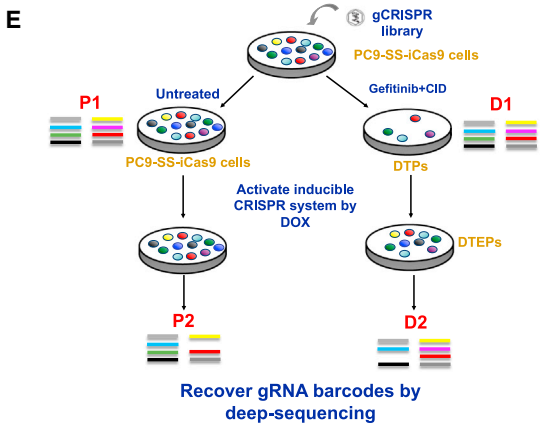

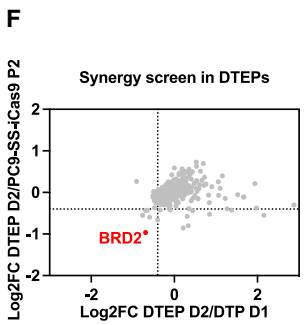

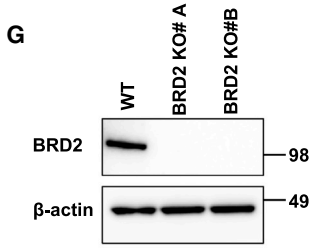

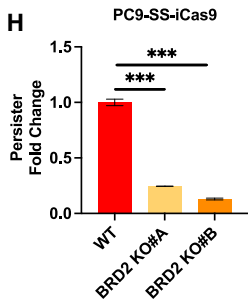

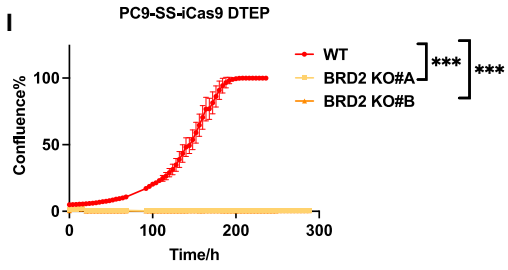

(legend on next page)

profiles, increased reliability on redox regulation, and enhanced stemness.[2,7,9–12] Despite our increasing understanding of DTPs in the last few years, limited efforts have been devoted to translating this concept into novel therapeutic strategies.

Combining a treatment controlling the majority of the cancer population with a second drug targeting DTPs holds the promise to delay or even prevent relapse.[13] DTPs have been shown to be vulnerable to ferroptosis induction. However, ferroptosis inducers, including RSL3 and ML210, cannot be used *in vivo* due to toxicity and/or poor bioavailability. More recently, an aurora kinase B inhibitor was reported to delay relapse, but only in lung cancer.[14] Thus, there remains an urgent need for well-tolerated broadly acting agents that selectively eliminate DTPs. Here, by using CRISPR and compound screens, we identify acquired vulnerabilities of DTPs and validate these targets in *in vivo* models.

RESULTS

Compound screen identifies bromodomain and extraterminal domain (BET) inhibition as a vulnerability of DTPs

We used epidermal growth factor receptor (EGFR) mutant PC9 lung cancer cells treated with gefitinib as a model to study DTPs. Most cancer cell lines are heterogeneous, harboring pre-existing genetically resistant subclones in addition to cells that survive therapy through non-genetic mechanisms. To eliminate cells having pre-existing genetic resistance to therapy, we introduced an activatable suicide switch construct into PC9 cells. This construct encodes a caspase-9 fusion protein that can be induced to dimerize by the addition of a chemical inducer of dimerization (CID), driven by the promoter of the Ki67 gene (PC9-suicide switch cells [PC9-SS]). Because Ki67 is only expressed in proliferating cells, activation of the switch by the addition of CID will eliminate only proliferating cells, allowing for the enrichment of non- or very slow cycling DTPs.[15] These PC9-SS cells were treated with a lethal dose of gefitinib for 7 days followed by another 7 days of treatment with both gefitinib and CID to activate the SS. The addition of CID resulted in selective induction of apoptosis in genetically resistant PC9 cells, which proliferate even under continuous treatment with gefitinib (Figure 1A). Different cell morphologies were observed in the remaining DTPs, indicating heterogeneity within this population. After prolonged culture in the absence of drug, DTEPs resembled the original morphology and regained sensitivity to gefitinib treatment as seen in the parental population (Figures S1A and S1B). Bulk RNA sequencing (RNA-seq) of paired DTPs and parental PC9 cells confirmed enrichment of the metastasis EMT signature up in DTPs as previously reported (Figure S1C). Together, the results validate the DTP enrichment method used here.

It has been shown that DTPs have increased stress levels, which suggests that challenging them with an additional stress could be lethal. We used a stress-focused compound library (agents that target proteotoxic stress, metabolic stress, oxidative stress, DNA damage stress, mitotic stress, and senolytics),[16] with the aim of identifying compounds that can be used to eradicate DTPs/DTEPs. Senescent cells share properties with DTPs, suggesting that they may share vulnerabilities. We therefore included four arms in our compound screens: parental proliferating PC9 cells, alisertib-induced senescent cells, gefitinib-induced DTPs maintained in gefitinib, and DTEPs: gefitinib-induced DTPs cultured without gefitinib (Figure 1B). In total, 163 drugs were added to the cells in 15 different concentrations. By calculating the AUC (area under the curve) score we were able to quantify the sensitivity of cells in each treatment condition for individual drugs. As reported before, BCL family inhibitors selectively eliminated both senescent cells and persisters, whereas the ferroptosis inhibitor RSL3 killed PC9 DTEPs (Figure 1C; Table 1).[12,17] Using the effect size of RSL3 as a cutoff, we identified the previously reported histone deacetylase inhibitors, and three BET inhibitors, inhibiting bromodomain protein-mediated transcription, as top hits in the DTEP arm. For validation, we generated DTEPs using the EGFR inhibitors gefitinib and osimetinib. Treatment with three different BET inhibitors (NEO2734, ARV-771, and CC90010) selectively decreased the viability of both gefi-DTEPs and osi-DTEPs as compared to their proliferating parental cells (Figure 1D). In summary, the stress-focused compound library screen identified BET inhibitors as a potential therapeutic approach to eliminate persisters.

CRISPR-based persister screen identifies bromodomain-containing protein 2 (BRD2) as a vulnerability of DTEPs

To complement the small-molecule screen and to identify genes essential for the survival of persisters, we performed a loss-of-function genetic screen using the doxycycline-inducible CRISPR-Cas9 vector system in PC9-SS cells.[18] Due to the rareness of persisters and their consequential small numbers, we choose to use a kinome-scale library for this screen. In short, we established PC9-SS cells stably expressing doxycycline-inducible

Figure 1. Compound screen and CRISPR-based persister screen identified BRD2 as a vulnerability of DTEPs

(A) Schematic representation of DTP induction and generation of DTEPs in PC9-SS cells.

(B) Schematic of small-molecule screen on parental, senescent, DTP, and DTEP cells.

(C) Top hits were selected based on the therapeutic window of senescent (Senes)/DTEP vs. parental. The x axis represents log fold change of the AUC score (Senes/DTEP vs. parental). The y axis represents the AUC score of Senes/DTEP cells.

(D) CellTiter blue quantification of relevant viability of parental cells or DTEPs (osimertinib and gefitinib induced) treated with BET inhibitors.

(E) Schematic of CRISPR-based kinome-wide genetic screen on DTEPs (n = 3 for each arm).

(F) Top hits were selected based on the fold depletion of sgRNAs DTEP vs. parental. Genes with 4 sgRNA dropped out were identified as hits.

(G) Western blot of BRD2 and β-actin in PC9-SS-iCas9 wild-type (WT) and BRD2^{KO} clones.

(H) Relative fold change of persisters number based on cell counting obtained from WT and BRD2^{KO} clones after 14 days of osimertinib exposure.

(I) IncuCyte-based proliferation of DTEPs of WT and BRD2^{KO} clones.

Error bars in (D), (H), and (I) represent mean ± SD, n = 3 independent experiments. Statistical significance was calculated by 2-tailed Student's t test (*p ≤ 0.05; **p ≤ 0.01; ***p ≤ 0.001).

Table 1. AUC values of compound screen

Drug name	Parental	DTP	DTEP	Senescence
A-1155463	2.96	2.06	1.49	0.33
Navitoclax	2.23	1.08	1.4	1.19
ARV-771	2.99	2.7	1.77	2.73
Neo2743	2.92	2.55	1.98	2.55
CC-90010	2.79	2.56	1.93	2.71
KNK437	3.57	3.57	3.57	2.67
Pracinostat	1.9	0.93	1.32	2.55
SBI-0206965	3.24	2.88	3.18	2.82
GSK2334470	3.12	2.39	2.56	3.57
AZD-8055	1.61	0.9	1.05	2.1
Geldanamycin	2.31	2.27	2.07	1.88
Givinostat (hydrochloride monohydrate)	1.68	0.7	1.18	2.49
Ixazomib	0.54	0.5	0.25	0.22
Nedisertib	3.28	2.39	3.57	3.3
BPTES	3.57	3.57	3.57	3
Vorinostat	2.42	1.54	1.79	3.38
Fisetin	2.79	2.66	2.97	2.22
trans-C75	2.78	2.84	2.46	2.52
ONC201	3.63	3.48	3.46	3.48
APY29	2.99	3.03	2.86	2.66
16F16	3.04	2.79	2.41	3.57
Tanespimycin	0.88	0.76	0.39	1.17
XL 413	3.57	3.57	3.57	3.26
PD0166285	1.55	1.39	1.74	1.24
Talazoparib	2.42	2.35	2.28	2.37
Carboplatin	3.57	3.56	3.57	3.34
Quercetin	2.46	2.4	2.9	1.88
(S)-Crizotinib	3.13	2.75	2.88	3.57
Ouabain (octahydrate)	1.73	1.81	1.51	1.76
4Œ°8C	3.57	3.57	3.57	3.57
GSK2656157	3.57	3.57	3.57	3.57
MKC3946	3.57	3.57	3.57	3.57
Nelfinavir	3.57	3.57	3.57	3.57
RAD51 inhibitor B02	3.57	3.57	3.57	3.57
V-9302	2.12	2.14	1.79	2.43
Danusertib	1.65	1.41	1.27	2.39
Tunicamycin	2.09	1.97	2.04	2.41
Panobinostat	0.47	0.11	0.19	1.29
Adavosertib	1.31	1.16	1.12	1.85
Garcinol	2.37	2.38	2.25	2.73
AZD-7762	1.12	1.11	1.05	1.45
Simurosertib	1.62	1.5	1.33	2.29
DHEA	3.02	2.87	2.97	3.57
MK-5108	2.13	2.1	1.82	2.86
KW-2478	1.68	1.73	1.97	1.74
Sabutoclax	2.23	2.25	2.28	2.58
PKM2-IN-1	2.29	2.28	2.14	2.88
kira6	2.72	2.38	3.28	2.95

(*Continued on next page*)

Table 1. *Continued*

Drug name	Parental	DTP	DTEP	Senescence
GSK-923295	2.47	2.57	2.1	3.23
Niraparib	2	2.08	1.93	2.48
AT9283	1.2	1.15	1.03	1.93
Oprozomib	0.56	0.76	0.45	0.99
NCT-503	2.98	3.57	3.1	2.81
U-104	3.06	3.04	3.12	3.57
D9	2.71	2.87	2.24	3.57
IITZ-01	1.21	0.92	0.73	2.54
ABT-737	2.98	2.62	3.57	3.31
CGK733	3.25	3.57	3.19	3.57
5-Fluorouracil	2.91	3.57	2.77	3.02
BIIB021	1.25	1.21	1.11	2.13
BAY-876	2.69	2.68	2.69	3.43
Auranofin	2.19	2.35	1.86	3.11
KU-60019	3.05	3.27	3.07	3.57
Mirin	2.84	2.87	2.84	3.57
Indisulam	1.61	1.95	1.4	2.25
Torin 2	0.65	0.45	0.36	1.94
OSU-03012	2.24	2.55	2.23	2.88
Oxaliplatin	2.57	2.95	2.45	3.27
DC661	1.9	2.06	1.87	2.74
CCT241533 (hydrochloride)	2.95	3.33	2.97	3.57
MKT 077	2.5	2.43	2.57	3.57
Berzosertib	1.64	1.76	1.3	3.04
CCT245737	2.2	2.51	1.71	3.57
Cisplatin	2.67	2.88	2.75	3.57
BMS-303141	2.77	3.57	2.37	3.57
Rabusertib	1.94	2.39	1.65	2.98
PD 407824	2.34	2.47	2.2	3.57
CCF642	1.89	2.19	1.6	3.11
Telaglenastat	1.9	2.79	1.58	2.58
NSC 109555	3.15	3.57	3.57	3.57
Doxorubicin (hydrochloride)	1.37	1.41	1.2	2.97
SCH900776	1.47	2.01	1.17	2.7
Daunorubicin (hydrochloride)	1.24	1.41	1.05	2.78
LY3177833	3.04	3.57	3.57	3.57
HA15	2.84	3.57	2.98	3.57
Ceralasertib	2.12	2.52	1.93	3.57
Alisertib	0.74	1.09	0.62	2.18
GDC-0575 dihydrochloride	1.12	1.66	0.67	2.71
(E)-Daporinad	0.29	0.74	0.5	1.37
Barasertib-HQPA	1.29	1.4	1.19	3.08
Rigosertib	0.53	0.85	0.42	2.46
Venetoclax	2.32	2.79	2.79	3.57
BAY-1895344 (hydrochloride)	0.75	1.44	0.66	2.41
GSK-1070916	0.4	0.73	0.3	2.75
CMPD1	1.88	2.56	2.11	3.57
GSK2194069	2.54	3.57	3.57	3.09

(*Continued on next page*)

Table 1. *Continued*

Drug name	Parental	DTP	DTEP	Senescence
Empesertib	1.05	1.38	0.88	3.57
Volasertib	0.32	0.55	0.23	3.57
(−)-Epigallocatechin gallate	2.9	NA	3.15	NA
(S)-Monastrol	2.85	2.85	2.52	NA
3-AP	3.12	3.08	3.12	NA
5-Azacytidine	2.41	3.57	2.49	NA
5-Methyl-1H-pyrazol-3(2H)-one	3.57	3.26	NA	NA
A-485	2.49	2.04	2.53	NA
Acetazolamide	NA	3.56	3.57	NA
Alvespimycin (hydrochloride)	0.25	NA	NA	1.14
AMG 900	NA	NA	NA	NA
Apcin	3.57	3.57	NA	3.57
AZD-5991	3.29	1.15	3.57	NA
AZD0156	3.57	2.76	2.79	NA
AZD1390	3.57	3.57	2.59	NA
AZD3965	3.57	3.57	NA	3.57
Bafilomycin A1	NA	NA	NA	NA
BAY1217389	0	NA	NA	3.57
BI 2536	NA	NA	NA	3.57
BML-277	3.05	2.98	2.65	NA
Bortezomib	NA	NA	NA	NA
Carfilzomib	NA	0.05	0	1.06
Cariporide	3.57	3.57	NA	3.57
Chloroquine (diphosphate)	NA	3.57	3.57	3.57
Daidzin	3.57	NA	3.54	NA
Dapagliflozin	3.57	NA	3.57	2.05
Decitabine	1.49	2	0.58	NA
Devimistat	3.34	NA	3.57	2.7
DTP3 (TFA)	3.57	3.57	NA	NA
Enasidenib	3.38	3.57	3.57	NA
Epothilone B	NA	NA	0	NA
Etoposide	2.16	2.31	1.98	NA
Filanesib	0	NA	NA	2.59
Gemcitabine	NA	1.27	NA	NA
GSK2606414	3.57	3.57	NA	3.57
GSK461364	NA	NA	NA	2.28
Hydroxychloroquine sulfate	3.57	NA	NA	NA
IACS-10759	0.84	NA	0.75	0.21
IPI-3063	3.36	2.89	3.42	NA
Ispinesib	NA	NA	NA	2.74
ISRIB (*trans*-isomer)	3.57	3.57	3.57	NA
L-Buthionine-(S)	2	3.57	3.57	3.57
Litronesib	0	NA	NA	NA
Luminespib	NA	NA	0	0.39
Marizomib	NA	NA	NA	NA
MRT68921 (dihydrochloride)	2.5	3.05	2.2	NA
ND 646	2.68	NA	3.57	NA
Olaparib	3.07	2.88	3.57	NA

(*Continued on next page*)

Table 1. *Continued*

Drug name	Parental	DTP	DTEP	Senescence
Paclitaxel	NA	NA	NA	1.55
pevonedistat (MLN4924)	1.86	1.86	1.67	NA
PF 3644022	3.57	2.45	3.07	NA
Prexasertib	NA	NA	0	NA
ProTAME	3.1	3.57	3.57	NA
PX-12	3.24	NA	2.99	NA
QNZ	0.92	2.32	NA	1.2
Quisinostat	NA	0.31	NA	1.24
Rapamycin	2.33	1.7	1.86	NA
RI-1	NA	NA	3.57	NA
Romidepsin	2.07	NA	0	0
RSL3	2.53	2.18	1.7	NA
Rucaparib	3.42	3.57	NA	3.57
SB-743921	NA	NA	NA	2.73
SC75741	2.33	2.61	2.32	NA
STF-083010	NA	NA	3.57	NA
TH588	3.4	3.52	3.57	NA
Thapsigargin	NA	NA	0	NA
Tozasertib	1.33	1.32	1.05	NA
ULK-101	3.57	NA	3.57	NA
Vinblastine (sulfate)	NA	NA	0	1.68
Vincristine (sulfate)	NA	NA	NA	2.07
VX 984 (M9831)	3.51	3.57	3.57	NA
YM-155	NA	NA	NA	0.15

Table 1 is related to Figure 1. NA, not applicable.

Cas9 (PC9-SS-iCAS9) (Figures S2A–S2C). The lentiviral-kinome single-guide RNA (sgRNA) library was transduced into proliferating PC9-SS-iCas9 cells followed by selection with puromycin for lentiviral integration. As described above, sgRNA-expressing PC9-SS-iCas9 cells were treated with gefitinib and CID for DTP induction and enrichment. After this, doxycycline was added to activate the Cas9-mediated genome editing (Figure 1E). Persisters were cultured for 10 days in doxycycline-containing medium without gefitinib to allow the depletion of cells containing sgRNAs targeting genes required for DTEP survival. Proliferating cells were used as a control in this screen. By identifying the sgRNAs specifically depleted in DTEPs as compared to proliferating cells, we identified vulnerabilities of DTEPs. Based on this criterion, the BET domain containing protein BRD2 was identified as a top hit in the genetic screen (Figure 1F). Two BRD2 knockout clonal PC9 cell lines were established for validation (Figure 1G). Knockout of BRD2 dramatically decreased the number of DTPs that survived osimertinib treatment (Figure 1H). Although the loss of BRD2 has hardly any effect on parental PC9 cell proliferation, it abolished the outgrowth of DTEPs in both IncuCyte proliferation assays and colony-formation assays (Figures 1I, S2D, and S2E). At this moment, there are no specific inhibitors for individual members of the BET family of proteins. To address in more detail which BET proteins are vulnerabilities of DTPs, individual knockdown of BRD2, BRD3, and BRD4 were performed in both EGFR mutant PC9 and BRAF mutant A375 to investigate their potential functions in DTP regulations. Bromodomain testis-specific protein was excluded from this experiment because it has been reported to be expressed in testis only, which is also confirmed in our RNA-seq data, given the limited read counts (<10) detected. Of note, BRD2 was the most abundantly expressed in PC9 as compared to the other BET proteins (Figure S3A). Among the three BET proteins we tested, BRD2 knockdown drastically suppressed the formation of DTPs in both PC9 and A375, whereas BRD3 knockdown has a minor/moderate effect on DTP emergency. Surprisingly, BRD4 knockdown confers resistance to osimertinib treatment as reflected by an increased number of DTPs surviving after 14 days of drug exposure (Figures S3B–S3E). Our findings on BRD4 are consistent with a recently published study on the embryonic-like diapause-like adaption that promoted tumor persistence associated with MYC suppression.[19] In the study, pharmacological suppression of BRD proteins with JQ1-induced diapause-like profiles and reduced the effect of cytotoxic treatment in cancer cells.[20,21] The overlap between the CRISPR screen and compound screen identifying BET proteins as vulnerabilities of persister cells highlights that the inhibition of BET proteins can serve as a promising strategy to selectively target DTEPs.

To further study the effects of BET inhibition on the proliferation of both parental PC9-SS cells and their DTEPs, we used IncuCyte live cell imaging to study cell proliferation. As reported

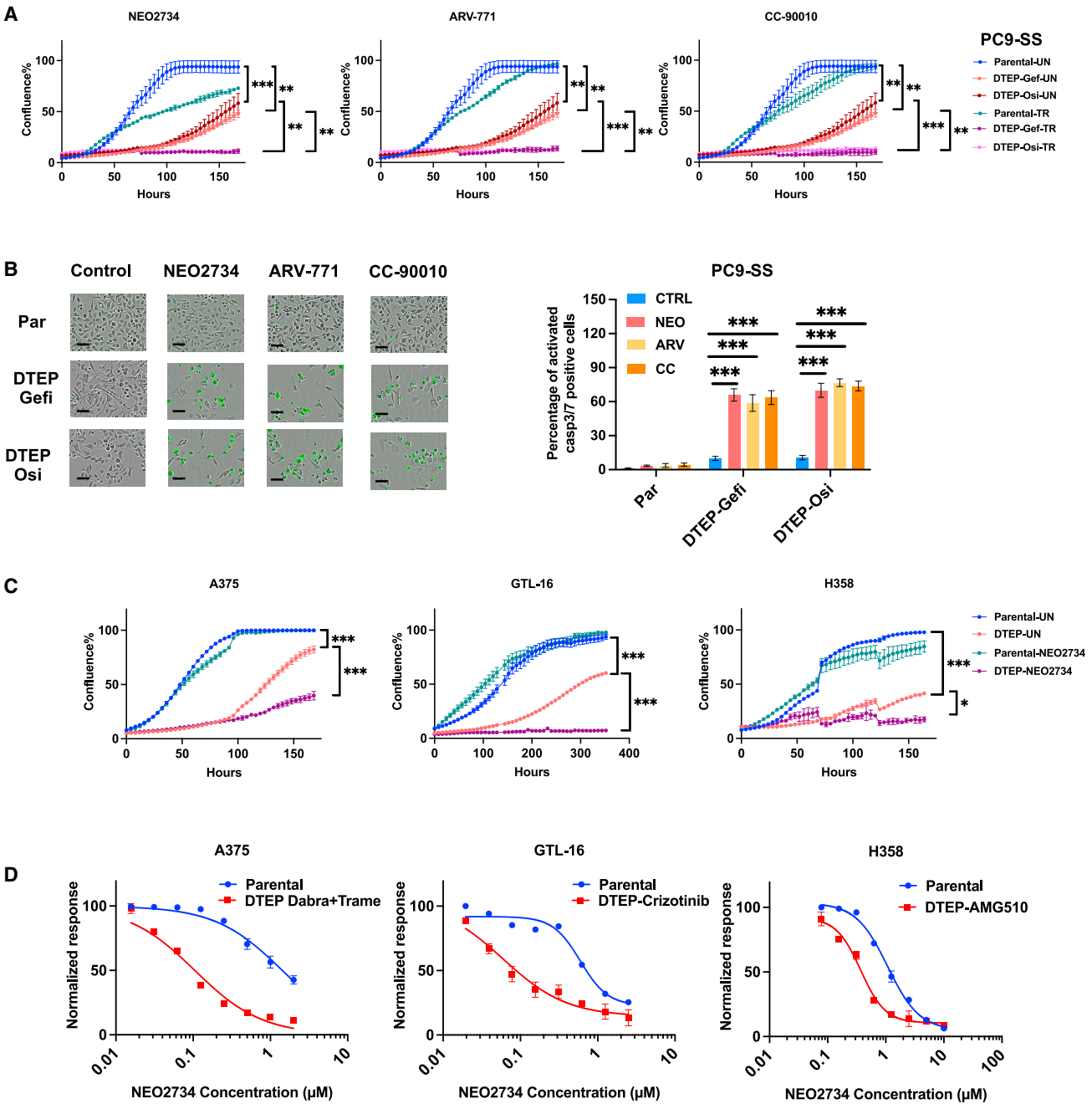

Figure 2. BET inhibition selectively triggered apoptotic cell death in EGFR inhibition (EGFRi)-induced persisters in lung cancer and eliminated DTEPs in a broad spectrum of cancer types

(A) IncuCyte-based proliferation of parental and DTEPs treated with BET inhibitors (n = 3).

(B) Caspase-3/-7 staining images and quantification of parental PC9 cells and DTEPs treated with BET inhibitors or DMSO at 72 h. Black scale bar, 100 μm.

(C) CellTiter blue quantification of relevant viability of parental cells or DTEPs (A375, GTL-16, and H358) treated with BET inhibitors.

(D) IncuCyte-based proliferation of parental and DTEPs (A375, GTL-16, and H358) treated with NEO2734.

Error bars in (A)–(D) represent mean ± SD, n = 3 independent experiments. Statistical significance was calculated by 2-tailed Student's t test (*$p \leq 0.05$; **$p \leq 0.01$; ***$p \leq 0.001$).

before, DTEPs induced in our system indeed exhibit a much slower proliferation rate as judged by both IncuCyte- and long-term colony-formation assays (Figures 2A and S4). BET inhibitors abolished DTP outgrowth into DTEPs while having minor effects on proliferating cells (Figures 2A and S4). Moreover, upon treatment with BET inhibitors, we observed a strong increase

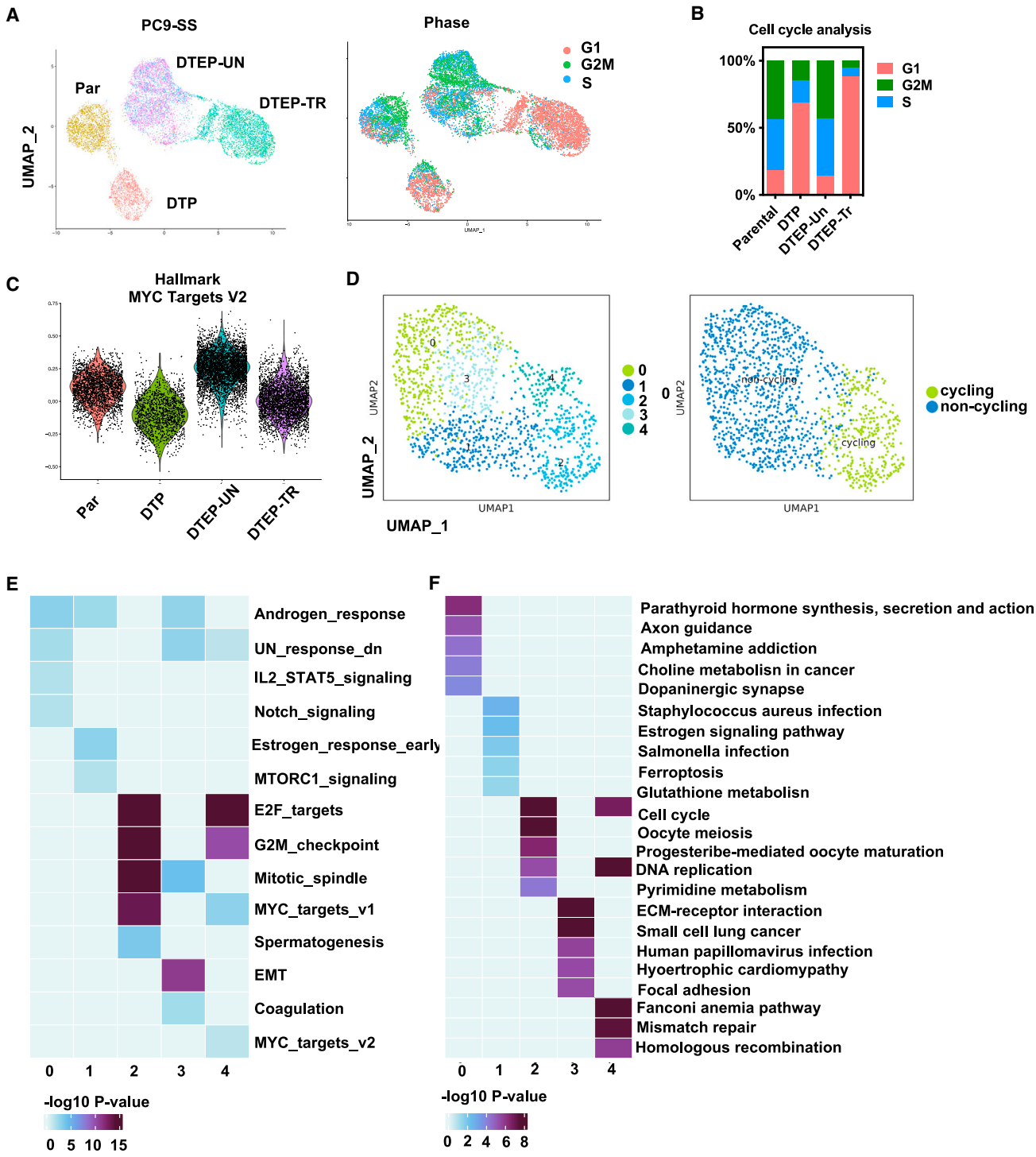

Figure 3. scRNA-seq uncovered distinct transcriptomic landscapes in parental, DTP, and DTEP cells

(A) Uniform manifold approximation and projection (UMAP) representation of scRNA-seq on parental, DTP, DTEP-untreated (DTEP-UN), and DTEP-treated with NEO2734 (DTEP-TR). Cells are colored based on different treatment conditions (left). Cells are colored based on different cell-cycle stages (right). (For DTEP-UN and DTEP/TR, samples were collected at 24 h [T1] and 48 h [T2]. T1 and T2 were analyzed as duplicates).

(B) Quantifications of cell-cycle phase for cells in parental, DTP, DTEP-UN, and DTEP-TR.

(C) Comparison of Myc targets module scores on parental, DTP, DTEP-UN, and DTEP-TR.

(legend continued on next page)

in the percentage of apoptotic cells in DTEPs as measured by caspase-3/-7-activated dye, accompanied by fragmentation into apoptotic bodies, indicating BET inhibitor-induced apoptotic cell death (Figure 2B).

BET inhibition eliminates DTEPs of a range of cancer types

We next investigated the effect of BET inhibition in several different tumor models, including A375 BRAF mutant melanoma, GTL-16 MET-amplified gastric carcinoma, and H358 KRAS^{G12C} mutant lung cancer cells, which were turned into DTPs by treatment with dabrafenib plus trametinib, the MET inhibitor crizotinib, and the KRASG12C inhibitor AMG510, respectively. BET inhibitor treatment of DTEPs derived from these three additional models was consistently lethal as reflected by IncuCyte proliferation assay and long-term colony-formation assay (Figures 2C, 2D, S4, and S5). Again, persisters derived from these cancer cell lines exhibited a slow proliferation rate and regained sensitivity to primary treatment after drug removal (Figures 2C and S1D). For all four models, we also tested RSL3 (GPX4 inhibitor) and ABT263 (BCL family inhibitor) with established activity toward DTPs. ABT263 only suppressed osi-DTEPs in PC9. No therapeutic window was observed for RSL3 in H358 G12C mutant lung cancer cells (Figure S6). Together, these findings support the observation that BET inhibitors suppressed DTEPs in a broader spectrum of cancer types than the presently identified drugs.

Single-cell RNA-seq (scRNA-seq) uncovers distinct transcriptomic landscapes in parental, DTP, and DTEP cells

To gain insight into the heterogeneity of persisters and to investigate the mechanism underlying the selective sensitivity of DTEPs to BET inhibition, we performed scRNA-seq. Seurat clustering and Dimplots were applied to identify the different clusters and visualization of the dimensional reduction. We compared single cells from four conditions: parental PC9, DTPs, DTEPs, and DTEPs treated with BET inhibitor. scRNA clustering uncovered distinct transcriptomic landscapes for parental, DTP, DTEP, and DTEP treated with NEO2734 (Figures 3A and S7; Table S1). DTPs are arrested in their cell cycle, whereas drug removal enables them to re-enter the cell cycle. BET inhibitor treatment increased the cell-cycle arrest in persisters (Figures 3A and 3B). The effect of BET inhibition on persisters could be confirmed further by the dynamic changes in MYC and E2F targets and apoptosis gene signaling in different clusters and decreased cell percentage arrested in G2/M (Figures 3A–3C and S7B).

In addition, scRNA seq confirmed the increase in stemness features reflected by the enrichment of hedgehog signaling (Figure S7C). Other previously reported biological features such as increases in reactive oxygen species (ROS) and active inflammatory responses, including interleukin-6-Janus kinase-STAT3 (IL-6-JAK-STAT3) signaling, interferon-α, and interferon-γ, were also enriched in DTPs (Figure S7C). To address whether different subpopulations exist within persisters, we performed Seurat clustering focusing on the DTP group only (Figures 3D–3F). In total, five clusters of DTPs were identified with subtle differences (Figure 3D). Analysis of their cell-cycle status showed that clusters 0, 1, and 3 belong to non-cycling persisters, whereas cycling persisters are present in clusters 2 and 4 (Figure 3D). Cluster 0 was marked by the enrichment of inflammatory signaling, including IL-2-STAT5 signaling, altered metabolism of choline metabolism in cancer, and enhanced stemness features reflected by notch signaling. Cluster 1 DTPs were marked by altered cellular metabolism, including ferroptosis and glutathione metabolism and protein synthesis reflected by mammalian target of rapamycin (mTOR) complex 1 signaling. This also supports the notion that non-cycling persisters are more vulnerable to ferroptosis inhibition.[4] EMT, coagulation, extracellular matrix-receptor interaction, and focal adhesion signaling were enriched in non-cycling persisters of cluster 3, indicating that these subpopulation of persisters may share a distinct cellular morphology. For the cycling persisters clusters 2 and 4, the common signaling features compared to non-cycling counterparts were cell-cycle-associated pathways, including E2F targets, G2M checkpoints, and DNA replication. Moreover, cluster 2 cycling persisters were marked by pyrimidine metabolism, and cluster 4 was marked by mismatch repair and homologous recombination. Analysis of their most representative hallmarks uncovered distinct biological features of the clusters, pointing at the complexity of DTPs even when derived from the same cancer type (Figures 3E and 3F).

To investigate the similarity among persisters with different tissue origins, transcriptome analysis was performed in four paired DTPs vs. parental cells. Pathway analysis (Hallmark gene sets and Kyoto Encyclopedia of Genes and Genomes [KEGG] gene sets) of differentially expressed genes in persisters as compared to parental proliferating cells uncovered their distinct biological features (Figure S8). As reported, DTPs are in a cell-cycle-arrested state as reflected by the suppression of both MYC and E2F targets. Ribosome, aminoacyl tRNA biosynthesis, and mTOR signaling are suppressed in DTPs as well, indicating that non-essential translation processes were less active in persisters.[22] Glycolysis was suppressed while enrichment was observed in bile acid metabolism, fatty acid metabolism, and adipogenesis, confirming altered metabolism in DTPs.[11,23] Apart from H358, in PC9, A375, and GTL-16, enrichment was also observed in gene sets, including inflammatory response, IL6-JAK-STAT3 signaling, and tumor necrosis factor-α signaling via NF-κB, interferon-γ, and interferon-α response, raising the possibility that active inflammation signaling may contribute to the suppression of drug responses in persisters. Other established features of persisters, including apoptosis, ROS pathway, and EMT transition, were also observed consistently by RNA-seq.[10] To comprehensively investigate the difference of persisters derived from multiple cancer origins, we defined each signature

(D) UMAP presentations of 5 clusters identified within DTPs. (Left) UMAP representations of cycling and noncycling counterparts within DTPs. (Right) Cycling: G2; noncycling: G1 and S).

(E and F) Heatmap summary of representative gene signatures (Hallmark [E] and KEGG [F]) for different clusters within the DTP subset. Color bar indicates −log10 p value.

enrichment score as a characteristic of every DTP dataset and calculated the distance between every pair of two samples based on the average value of differences over all characteristics (Table S2; see STAR Methods). The average distance of H358-DTPs gene signature to the three other DTPs is the longest observed, indicating the dissimilarity of H358-DTPs to the other DTPs (Figure S8C).

DTPs share some features with senescent cells but have different vulnerabilities

Previously, it was reported that a senescence-like dormant state can be triggered in PC9 cells by the combination of EGFR and MEK inhibition.[7] Consistent with these findings, DTPs with an enriched senescence signature were found in clusters 0, 1, and 2 based on our scRNA data (Figure S9A). In addition, we observed enrichment of the FRIDMAN senescence gene signature in our bulk RNA-seq data (Figure S9B). Moreover, the similarities between persisters and senescent cells are further supported by the observation that a fraction of the persisters stained positive for senescence-associated β-galactosidase (Figure S9C).

Previously, our group reported that the inhibitor of extrinsic apoptosis signaling cFLIP is a vulnerability of senescent cancer cells and that the DR5 agonist conatumumab is a broadly acting senolytic agent.[18] However, in the context of persister cancer cells, the overexpression of cFLIP did not have an effect on the emergence of DTPs and could only partially rescue the killing of DTEPs by BET inhibitors (Figures S9D and S9E). Moreover, alisertib-induced senescent cancer cells are more vulnerable to conatumumab as compared to persisters (Figure S9F). Transcriptomic analysis also suggested that NF-κB targets are selectively increased in persisters compared to senescent cells (Figure S9G). Collectively, these data indicate that despite the similarity of persisters and senescent cells in some aspects, they display distinct vulnerabilities. Moreover, the mRNA expression of BRD2, BRD3, and BRD4 remained unchanged in DTPs, indicating that the suppressive effect of BET inhibitors on persisters cannot be attributed to increased BRD protein expression (Figure S3A).

scRNA-seq identifies lethal levels of ROS in DTEPs after BET inhibition

Most interesting with respect to the observed sensitivity of DTEPs to BET inhibitors, we also observed dynamic changes of ROS gene sets in different clusters (Figure 4A). Recently, redox homeostasis has been implicated in features of DTP cells, including epigenetic regulation of slow cell proliferation status, adaptive metabolism alteration, and tumor cell plasticity.[24] In line with this notion, ROS signaling was increased during DTP formation and decreased again after drug washout and when DTPs started to proliferate into DTEPs. DTEPs treated with BET inhibitors failed to alleviate ROS levels, leading to the hypothesis that BET inhibition may eliminate DTEPs by increasing the intracellular ROS to a lethal level. Flow cytometry-based staining enabled us to quantify ROS levels in different conditions. Increased intracellular ROS levels were observed in both lung cancer and melanoma DTPs (Figures 4B and 4C). The intracellular ROS level dropped in DTEPs, whereas treatment with both the known ROS inducer RSL3 and NEO2734 increased ROS levels in DTEPs (Figures 4B and 4C). Moreover, the addition of a general ROS scavenger, *N*-acetylcysteine (NAC), rescued DTEPs from BET inhibitors, further supporting that the lethal effect BET inhibitors have on DTEPs can be attributed to increased ROS levels in DTEPs (Figure 4D, left panel). Similar results were obtained from A375 melanoma cells and GTL-16 gastric cancer cells (Figures 4E, S10, and S11). Consistently, BRD2 knockdown also increases ROS levels in DTPs in both PC9-SS and A375 cells (Figures S10C and S10D). Previously DTPs were reported to be vulnerable to ferroptosis induction.[17] To investigate which type of cell death was induced by BET inhibition, we performed rescue experiments using a ferroptosis inhibitor ferrostatin and an apoptosis inhibitor, Z-VAD-FMK. In PC9, Z-VAD-FMK partially rescued DTEPs from BET inhibition, whereas ferrostatin had no effect, supporting the induction of apoptosis in PC9 DTEPs upon treatment with BET inhibitors (Figure 4D, center and right panels). In A375 and GTL16, both Z-VAD-FMK and ferrostatin could partially rescue the inhibitory effect of BET inhibitors on DTEPs, indicating that different types of cell death were induced in these two models (Figures 4E and S11). Regarding H358-derived DTPs, BET inhibition failed to increase the ROS level (Figure S10). We also failed to observe a selective toxicity of DTPs to RSL3 (Figure S6). The different phenotypes observed here suggest that H358-DTPs may share fewer similarities with the DTPs derived from other cancer types, which was also supported by the heatmap analysis of the difference in biological features among four paired DTPs vs. parental samples (Figure S8C). The suppressive effects of BET inhibition on H358-DTPs may be attributed to the targeting of other vulnerabilities apart from ROS induction. The data shown above highlight the complexity and heterogeneity of DTPs from different tissue origins.

BET inhibition suppresses DTEPs through inhibiting anti-oxidative DTP markers, including glutathione peroxidase 2 (GPX2), microsomal glutathione S-transferase 1 (MGST1), and aldehyde dehydrogenase 3 family member A1 (ALDH3A1)

To investigate the mechanism by which BET inhibition induces ROS accumulation, we focused on DTP markers differentially expressed among identified Seurat clusters. Pathway analysis of downregulated markers in DTEPs upon NEO2734 treatment identified their potential function in regulating cellular response to oxidative stress, cell motility, cell growth, extracellular matrix organization, and response to xenobiotic stimulus (Figures 5A and 5B). Consistent with our observations of further ROS induction in DTEPs upon treatment with BET inhibitors, three DTP markers with well-established anti-oxidative functions, including GPX2, ALDH3A1, and MGST1, were strongly suppressed upon treatment with NEO2734 (Figures 5A, 5C, and 5D).[4,25,26] Stable knockdown of GPX2, MGST1, and ALDH3A1 significantly suppressed persister emergence and sensitized DTEPs to BET inhibition (Figures 5E and 5F). Moreover, increased ROS levels were observed in DTPs derived from GPX2, MGST1, and ALDH3A1 PC9 cells (Figure S12). In summary, our results suggest that BET inhibition kills DTEPs by inhibiting anti-oxidative DTP markers, including GPX2, MGST1, and ALDH3A1, thereby creating lethal ROS levels.

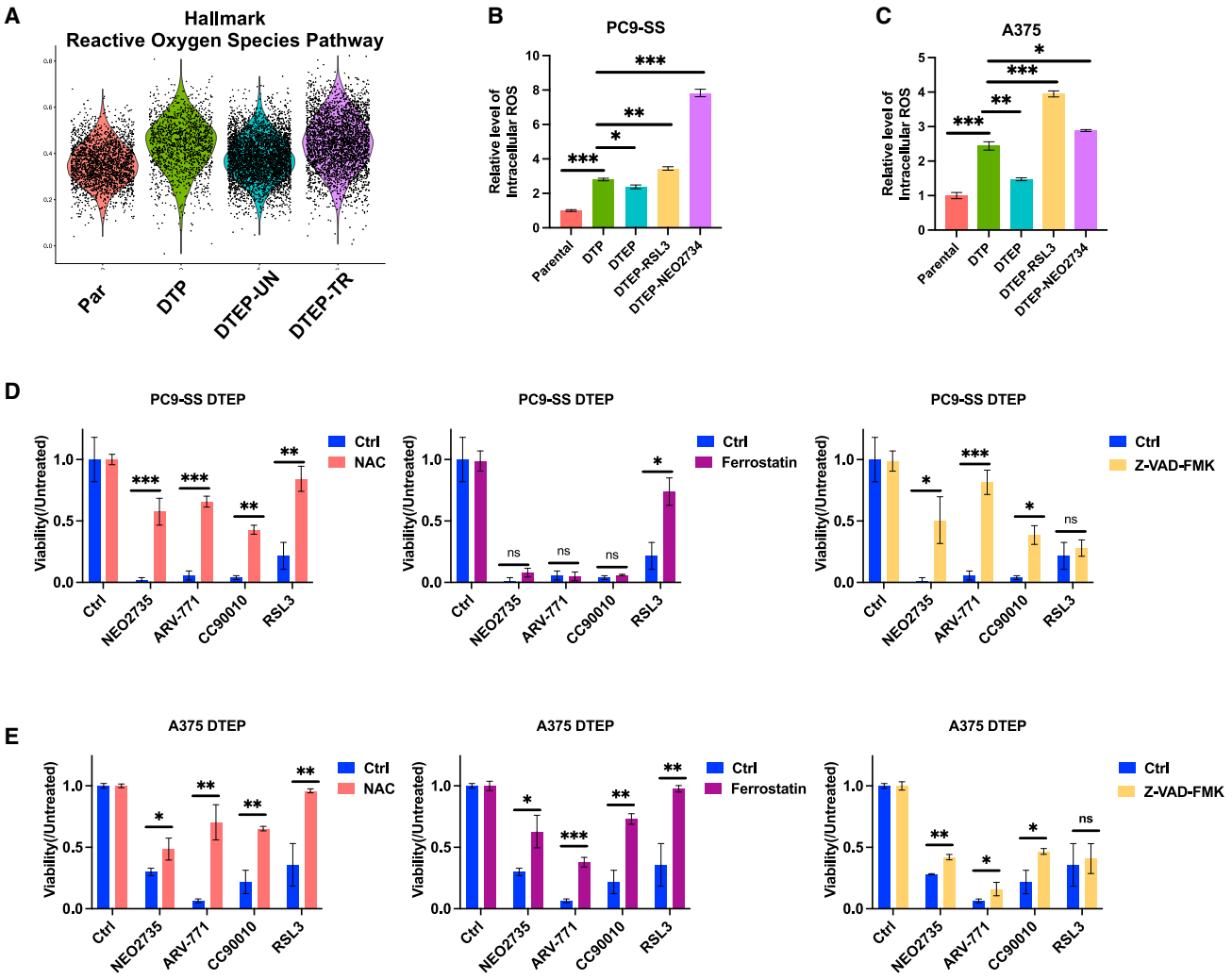

Figure 4. scRNA-seq identified lethal levels of ROS in DTEPs after BET inhibition

(A) Comparison of ROS pathway gene signature module scores on parental, DTP, DTEP-UN, and DTEP-TR.

(B and C) Flow cytometry-based quantification of intracellular ROS level (mean fluorescent intensity) in on parental, DTP, DTEP-UN, and DTEP-TR in both PC9 (B) and A375 (C) cells. (Samples collected at 72 h, NEO2734: 0.25 μM).

(D and E) Relative cell viability of DTEPs exposure to BET inhibitors with or without NAC, ferrostatin, and Z-VAD-FMK (NEO2734: 0.25 μM; NAC: 2.5 mM; ferrostatin: 2.5 μM; Z-VAD-FMK: 10 μM).

Error bars in (B)–(E) represent mean ± SD, n = 3 independent experiments. Statistical significance was calculated by 2-tailed Student's t test (ns, not significant; *p ≤ 0.05; **p ≤ 0.01; ***p ≤ 0.001).

BET inhibition suppresses DTEPs and delays tumor relapse *in vivo*

To date, most studies on DTPs have been performed *in vitro* and there are only limited data to support the notion that DTPs actually contribute to clinical therapy resistance. To test whether BET inhibition eliminates persisters *in vivo*, we performed animal experiments. In the first experiment, we engrafted PC9 lung cancer cells into immunocompromised mice. To obtain DTP populations *in vivo*, mice were treated with osimertinib continuously for 28 days. DTPs only represent a rare subpopulation of parental cancer cells, which is supported by the observation that after 28 days of treatment, tumor volumes drop to a range of 0.5–40 mm^3 (Figure 6A). After 28 days of DTP induction, mice were randomly assigned to subsequent treatment with either vehicle alone or BET inhibitor. The switch to vehicle allowed the regrowth of tumors, presumably from DTPs. In contrast, subsequent treatment with BET inhibitor suppressed DTEPs and delayed tumor relapse *in vivo* without apparent toxicity for mice, as analyzed by body weight (Figure 6A). Importantly, treatment with a single-agent BET inhibitor resulted in statistically insignificant growth suppression of parental PC9 cells (Figure S13A). Similar results were obtained in the A375 melanoma model. DTPs induced by continuous treatment with dabrafenib and trametinib for 28 days were sensitive to subsequent treatment with BET inhibitor, because such treatment significantly inhibited DTEP outgrowth as judged by the delay in tumor relapse. Again,

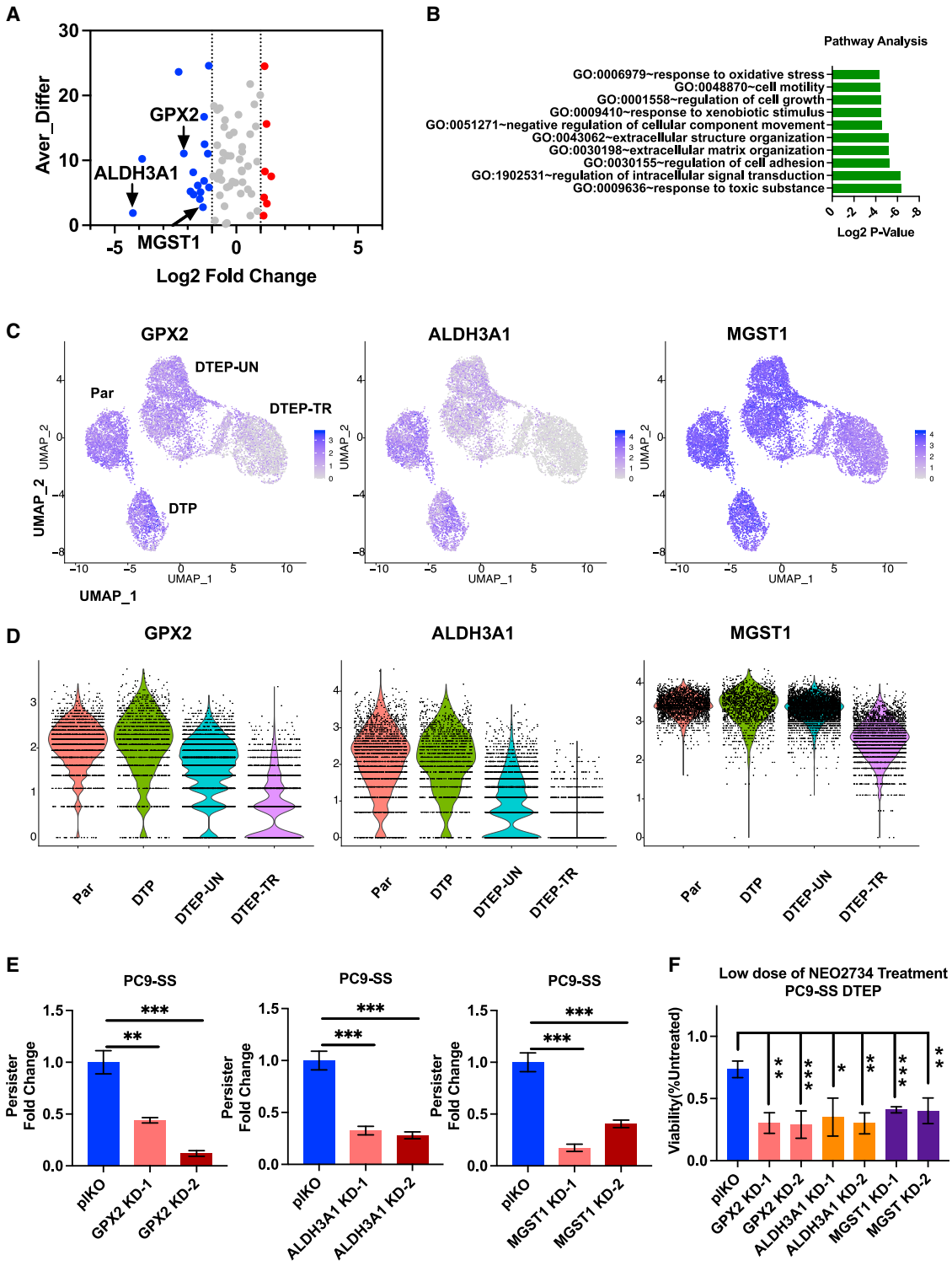

Figure 5. BET inhibition suppressed DTEPs through inhibiting antioxidative DTP markers, including GPX2, MGST1, and ALDH3A1

(A) Differentially expressed DTP markers in NEO2734 treated vs. untreated DTEPs. X axis: log2 fold change (DTEP-TR/DTEP-UN) based on bulk RNA-seq data; y axis: average difference calculated based on scRNA-seq data. Blue: downregulated; red: upregulated.

(B) Gene Ontology term enrichment analysis of 17 DTP markers downregulated upon NEO2734 challenged in DTEPs identified in Figure 4A.

(C) UMAP representation of GPX2, ALDH3A1, and MGST1 expressions in parental, DTP, DTEP-UN, and DTEP-TR. Color scale indicates the log2 counts per million per cell.

(legend continued on next page)

treatment with BET inhibitor did not significantly control the growth of parental A375 cells *in vivo* (Figures 6B and S13B).

To gain more insight into the roles of persisters and BET inhibition in resistance to treatment, we tried to establish spontaneous relapse xenograft models using PC9 and A375 cells treated with osimertinib or dabrafenib plus trametinib, respectively. However, for the PC9 *in vivo* model, osimertinib did not give rise to any spontaneous relapses, even after 4 months (data not shown). Therefore, we mimicked the process of spontaneous relapse by drug removal after 28 days of therapy. Due to tumor heterogeneity, DTPs are not likely to be induced synchronously. Therefore, we also used standard-of-care therapy and BET inhibitor in combination from the beginning. Up-front treatment with combinational therapy of osimertinib and BET inhibitor for 28 days significantly prolonged the time to tumor relapse after drug removal compared to the osimertinib monotherapy group, with no apparent toxicity observed in the animals (Figure 6C). More strikingly, in the A375 melanoma model, tumors gradually began to relapse starting from 40 days. However, triple treatment with BET inhibitor completely prevented spontaneous relapse without weight loss (Figure 6D). In summary, the *in vivo* results show that BET inhibition suppresses persisters directly in a sequential treatment and delayed tumor spontaneous relapse without any significant effect on the proliferation of the parental cell population. We conclude that co-treatment with BET inhibitor prolongs time to tumor relapse through killing drug-tolerant persisters.

DISCUSSION

It is generally believed that the DTP population serves as a reservoir from which genetically resistant clones can emerge.[2,9] Although mounting evidence supports the existence of DTPs in various cancer types, most studies in this field are performed *in vitro.* Thus, there is a need for evidence supporting the role of DTPs in cancer recurrence *in vivo*. Here, we used an unbiased approach to identify the largest vulnerabilities of DTPs and provide proof-of-concept in animal studies that the use of BET inhibitors either in a sequential therapeutic strategy or in an up-front combinational treatment can delay cancer recurrence in cancers of different tissues of origin. The drug synergy we observed here does not result from synergistic effects on the same cell populations, because BET inhibitors did not affect the growth of parental cells. That drug synergy can result from targeting different subpopulations of cancer cells was already suggested by others.[13]

DTPs are known to be vulnerable to ferroptosis induction.[17] Ferroptosis has been actively explored in the field as a promising strategy for anti-cancer treatment not only restricted to the eradication of DTPs. However, the preclinical drugs inducing ferroptosis by directly targeting GPX4 such as RSL3 and ML210 cannot be used *in vivo* due to toxicity, which may be explained by a recent finding that the increased sensitivity to ferroptosis induction has been observed in human hematopoietic stem cells (HSCs).[27] This raised concerns about the potential side effects that similar reagents may cause to hematopoiesis and HSC function. Ferroptosis was also described in neutrophils dampening the anti-cancer immune response and clinical outcome of immunotherapies.[28] Hence, more work is likely needed to exploit ferroptosis as a cancer treatment strategy.

In our study, we demonstrated that BET inhibitors eliminate persisters both *in vitro* and *in vivo,* delaying tumor recurrence with well-tolerated toxicity. Mechanistically, BET inhibition increases intracellular ROS to lethal levels by inhibiting DTP marker genes with anti-oxidative function, including GPX2, ALDH3A1, and MGST1. It has been shown before that DTPs are under high oxidative stress, making them more vulnerable to anti-oxidative regulation. The sources of the increased ROS in DTPs are still elusive, but they may be related to their altered metabolism. Using bulk RNA-seq and scRNA-seq, we uncovered that BET inhibitors specifically suppressed the anti-oxidative DTP markers, which caused a further accumulation of ROS. Oren et al.[4] reported the existence of both non-cycling and slowly cycling DTPs. GPX2 is preferentially expressed in slowly cycling DTPs, essentially for their maintenance, whereas RSL3-mediated ferroptosis induction could only selectively eliminate non-cycling persister cells. It has been demonstrated that MGST1 inhibits ferroptotic cancer cell death in pancreatic ductal adenocarcinoma.[25] By suppressing GPX2 and MGST1 simultaneously, BET inhibitors have the potential to eliminate both cycling and non-cycling persisters.

Cellular stress can lead to different cellular states such as senescence, dormancy, DTP state, and diapause.[2,7,19,29] However, to date, there is a lack of gold standard biomarkers to distinguish these states. In this study, we show that DTPs share similarities with senescent cells but have different vulnerabilities. Previously, our group uncovered the bystander effect of senescent cells to sensitize surrounding nonsenescent cells to senolytic treatment. Moreover, the senescence-associated secretory phenotype has been reported to promote cancer response to immune checkpoint inhibitors. In this study, we also found increased expression of secreted proteins in DTPs as compared to parental treatment-naive cells (Figure S7C). Based on transcriptomic data, we observed that DTPs preferentially enhanced the expression of intercellular cell adhesion molecule, chemokine (C-C motif) ligand 5, and inflammatory cytokine IL-6, which are essential for lymphocyte recruitment and immune cell activation (Figure S9G). Combinational treatments with standard-of-care therapy and immune checkpoint inhibitor have showed an

(D) Violin plots for GPX2, ALDH3A1, and MGST1 normalized reads in individual cells in parental, DTP, DTEP-UN, and DTEP-TR.
(E) Relative fold change of persisters number obtained from GPX2, ALDH3A1, and MGST1 knockdown cells after 14 days of osimertinib and CID exposure. pLKO empty vector-infected cells were used as a control.
(F) Relative cell viability of DTEPs upon treatment with NEO2734 (0.05 μM). DTEPs were derived from pLKO, GPX2, ALDH3A1, and MGST1 knockdown cells. pLKO empty vector-infected cells were used as a control.
Error bars in (E) and (F) represent mean ± SD, n = 3 independent experiments. Statistical significance was calculated by 2-tailed Student's t test (*$p \leq 0.05$; **$p \leq 0.01$; ***$p \leq 0.001$).

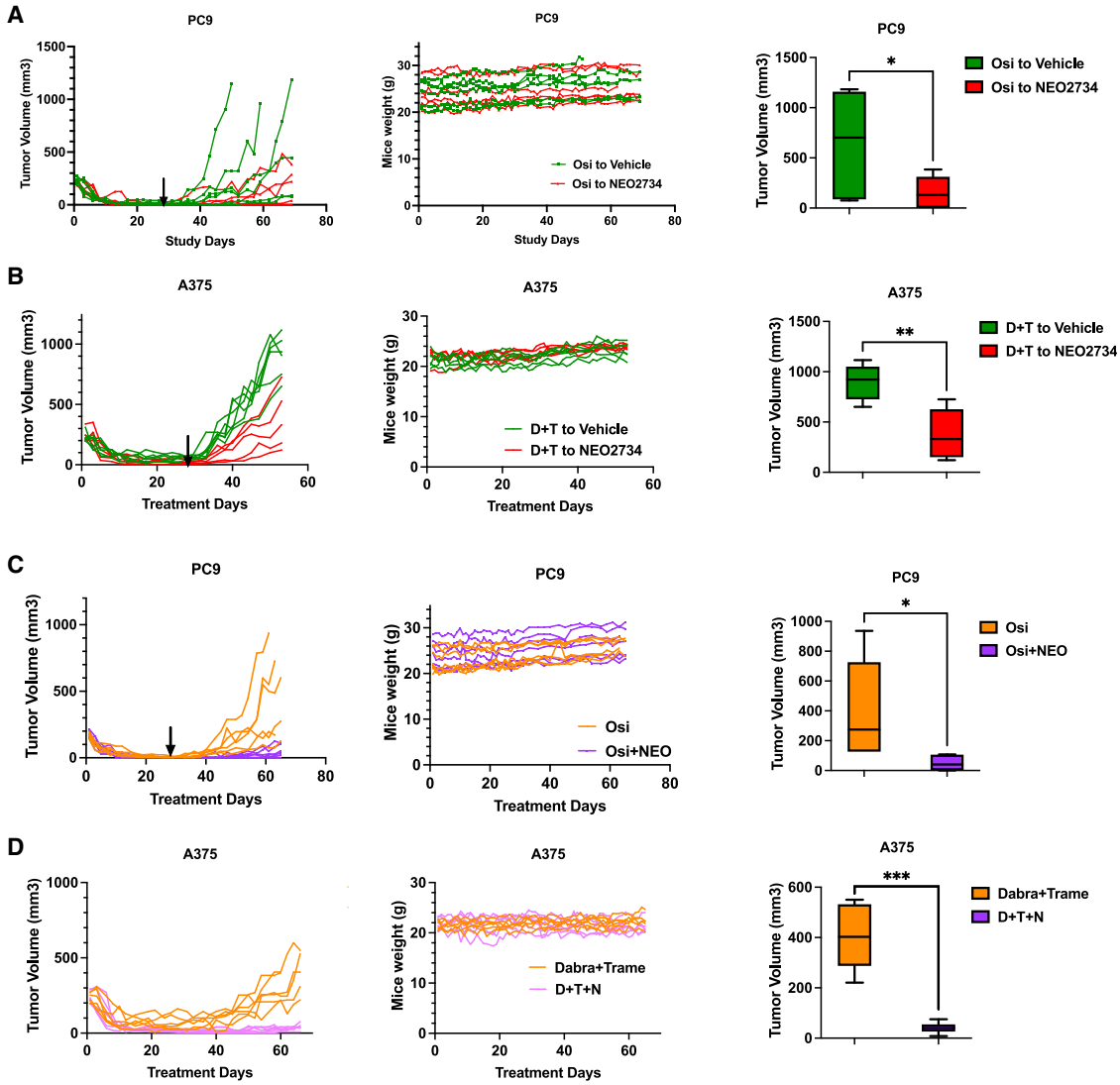

Figure 6. BET inhibitor suppressed DTEPs and delayed tumor relapse *in vivo* with a well-tolerated toxicity

(A) Relative tumor volumes and mice weights in sequential treatment groups with either vehicle or NEO2734 in PC9 subcutaneous-bearing mice. Mice were switched to vehicle or NEO2734 treatment at day 28 (n = 6 for each group) (osimertinib, 10 mg/kg once daily, and NEO2734, 4 mg/kg, 5 days/week).

(B) Relative tumor volumes and mice weights in sequential treatment groups with either vehicle or NEO2734 in A375 subcutaneous-bearing mice. Mice were switched to vehicle or NEO2734 treatment at day 28 (n = 6 for dabrafenib + trametinib to vehicle, n = 5 for dabrafenib + trametinib to NEO2734) (4 mg/kg NEO2734, 5 days/week; 30 mg/kg dabrafenib + 0.6 mg/kg trametinib daily).

(C) Relative tumor volumes and weights for PC9-bearing mice receiving osimertinib monotherapy or osimertinib + NEO2734 combination therapy. Treatments were stopped at day 28 (n = 6 for each group) (osimertinib, 10 mg/kg once daily, and NEO2734, 4 mg/kg, 5 days/week).

(D) Relative tumor volumes and weights for A375-bearing mice receiving combination treatment of dabrafenib (D) + trametinib (T) or triple treatment with NEO2734 (N). Mice were treated continuously (n = 6 for each group)) (4 mg/kg NEO2734, 5 days/week; 30 mg/kg dabrafenib + 0.6 mg/kg trametinib daily). Data are presented as mean ± SEM. Two-way ANOVA was applied for the *in vivo* study statistical analysis (*p ≤ 0.05; **p ≤ 0.01; ***p ≤ 0.001).

unexpected success clinically.[30] Future investigations into the potential effects of DTPs on shaping the tumor microenvironment may provide additional insights into how to best target DTPs to delay tumor relapse.

Limitations of the study

We performed a kinome-based genetic screen on DTPs to identify their vulnerabilities. The limited size of the library used was the consequence of the rareness of DTPs. As a consequence, we do not have a comprehensive overview of the vulnerabilities of DTPs from this experiment. A second limitation of the study is that there are no biomarkers to unambiguously identify DTPs *in vivo*. Hence, our conclusion that BRD inhibitor treatment delays relapse by eliminating DTPs cannot be verified directly *in vivo* and is based on our *in vitro* observations.

STAR★METHODS

Detailed methods are provided in the online version of this paper and include the following:

- KEY RESOURCES TABLE
- RESOURCE AVAILABILITY
  - Lead contact
  - Materials availability
  - Data and code availability
- EXPERIMENTAL MODEL AND STUDY PARTICIPANT DETAILS
  - Animal models
  - Cell line authentication
- METHOD DETAILS
  - Reagents
  - Drug treatments
  - Compound screen
  - CRISPR/Cas9-based genetic screen
  - RNA-sequencing and GSEA analysis
  - Single cell RNA sequencing
  - Plasmids
  - Cell viability measurement
  - Long term colony formation assays
  - Incucyte cell proliferation assays and caspase-3/7 activity monitoring
  - Lentiviral transductions
  - CRISPR mediated knockout of BRD2
  - Western Blotting and antibodies
  - RNA extraction and quantitative PCR (QPCR)
  - Senescence-associated β-galactosidase staining
  - Reactive oxygen species staining and flow cytometry
- QUANTIFICATION AND STATISTICAL ANALYSIS
  - Statistical analyses

SUPPLEMENTAL INFORMATION

Supplemental information can be found online at https://doi.org/10.1016/j.xcrm.2024.101471.

ACKNOWLEDGMENTS

We thank Victoria Wang for the kind gift of GTL-16 cells. We thank Frank van Gemert and Martijn van Baalen from the NKI Flow Cytometry Facility for their technical support. We thank Ming Wu from Bayer AG for her suggestion on scRNA analysis. This work was supported by grant no. 101007937 of the Innovative Medicines Initiative.

AUTHOR CONTRIBUTIONS

Conceptualization, M.C., L.W., R.L.B., and R.B. Investigation, M.C., S.M., C.L., A.V., I.d.R., C.Y., H.J.K., B.M., F.E., F.J., O.v.T., M.B., N.P., R.A.J., S.Q., H.J., J.C.K.v.d.M., and S.V. Resources, A.S., L.W., W.Q., R.L.B., and R.B. Methodology, M.C., L.W., R.L.B., and R.B. Formal analyses, M.C., C.L., A.V., I.d.R., and C.Y. Writing, M.C., R.L.B., and R.B. Funding acquisition, R.B. Supervision, L.W., R.L.B., and R.B.

DECLARATION OF INTERESTS

The authors declare no competing interests.

Received: June 2, 2023
Revised: December 1, 2023
Accepted: February 21, 2024
Published: March 19, 2024

REFERENCES

1. Dhanyamraju, P.K., Schell, T.D., Amin, S., and Robertson, G.P. (2022). Drug-Tolerant Persister Cells in Cancer Therapy Resistance. Cancer Res. *82*, 2503–2514. https://doi.org/10.1158/0008-5472.CAN-21-3844.
2. De Conti, G., Dias, M.H., and Bernards, R. (2021). Fighting Drug Resistance through the Targeting of Drug-Tolerant Persister Cells. Cancers *13*, 1118. https://doi.org/10.3390/cancers13051118.
3. Sharma, S.V., Lee, D.Y., Li, B., Quinlan, M.P., Takahashi, F., Maheswaran, S., McDermott, U., Azizian, N., Zou, L., Fischbach, M.A., et al. (2010). A chromatin-mediated reversible drug-tolerant state in cancer cell subpopulations. Cell *141*, 69–80. https://doi.org/10.1016/j.cell.2010.02.027.
4. Oren, Y., Tsabar, M., Cuoco, M.S., Amir-Zilberstein, L., Cabanos, H.F., Hütter, J.C., Hu, B., Thakore, P.I., Tabaka, M., Fulco, C.P., et al. (2021). Cycling cancer persister cells arise from lineages with distinct programs. Nature *596*, 576–582. https://doi.org/10.1038/s41586-021-03796-6.
5. Marsolier, J., Prompsy, P., Durand, A., Lyne, A.M., Landragin, C., Trouchet, A., Bento, S.T., Eisele, A., Foulon, S., Baudre, L., et al. (2022). H3K27me3 conditions chemotolerance in triple-negative breast cancer. Nat. Genet. *54*, 459–468. https://doi.org/10.1038/s41588-022-01047-6.
6. Shen, S., Vagner, S., and Robert, C. (2020). Persistent Cancer Cells: The Deadly Survivors. Cell *183*, 860–874. https://doi.org/10.1016/j.cell.2020.10.027.
7. Kurppa, K.J., Liu, Y., To, C., Zhang, T., Fan, M., Vajdi, A., Knelson, E.H., Xie, Y., Lim, K., Cejas, P., et al. (2020). Treatment-Induced Tumor Dormancy through YAP-Mediated Transcriptional Reprogramming of the Apoptotic Pathway. Cancer Cell *37*, 104–122.e12. https://doi.org/10.1016/j.ccell.2019.12.006.
8. Blakely, C.M., Pazarentzos, E., Olivas, V., Asthana, S., Yan, J.J., Tan, I., Hrustanovic, G., Chan, E., Lin, L., Neel, D.S., et al. (2015). NF-kappaB-activating complex engaged in response to EGFR oncogene inhibition drives tumor cell survival and residual disease in lung cancer. Cell Rep. *11*, 98–110. https://doi.org/10.1016/j.celrep.2015.03.012.
9. Tyner, J.W., Haderk, F., Kumaraswamy, A., Baughn, L.B., Van Ness, B., Liu, S., Marathe, H., Alumkal, J.J., Bivona, T.G., Chan, K.S., et al. (2022). Understanding Drug Sensitivity and Tackling Resistance in Cancer. Cancer Res. *82*, 1448–1460. https://doi.org/10.1158/0008-5472.CAN-21-3695.
10. Wilson, C., Nicholes, K., Bustos, D., Lin, E., Song, Q., Stephan, J.P., Kirkpatrick, D.S., and Settleman, J. (2014). Overcoming EMT-associated resistance to anti-cancer drugs via Src/FAK pathway inhibition. Oncotarget *5*, 7328–7341. https://doi.org/10.18632/oncotarget.2397.
11. Shen, S., Faouzi, S., Souquere, S., Roy, S., Routier, E., Libenciuc, C., André, F., Pierron, G., Scoazec, J.Y., and Robert, C. (2020). Melanoma Persister Cells Are Tolerant to BRAF/MEK Inhibitors via ACOX1-Mediated Fatty Acid Oxidation. Cell Rep. *33*, 108421. https://doi.org/10.1016/j.celrep.2020.108421.
12. Hata, A.N., Niederst, M.J., Archibald, H.L., Gomez-Caraballo, M., Siddiqui, F.M., Mulvey, H.E., Maruvka, Y.E., Ji, F., Bhang, H.e.C., Krishnamurthy Radhakrishna, V., et al. (2016). Tumor cells can follow distinct evolutionary paths to become resistant to epidermal growth factor receptor inhibition. Nat. Med. *22*, 262–269. https://doi.org/10.1038/nm.4040.
13. Palmer, A.C., and Sorger, P.K. (2017). Combination Cancer Therapy Can Confer Benefit via Patient-to-Patient Variability without Drug Additivity or Synergy. Cell *171*, 1678–1691.e13. https://doi.org/10.1016/j.cell.2017.11.009.
14. Criscione, S.W., Martin, M.J., Oien, D.B., Gorthi, A., Miragaia, R.J., Zhang, J., Chen, H., Karl, D.L., Mendler, K., Markovets, A., et al. (2022). The landscape of therapeutic vulnerabilities in EGFR inhibitor osimertinib drug

tolerant persister cells. NPJ Precis. Oncol. *6*, 95. https://doi.org/10.1038/s41698-022-00337-w.

15. Schepers, A., Jochems, F., Lieftink, C., Wang, L., Pogacar, Z., Leite de Oliveira, R., De Conti, G., Beijersbergen, R.L., and Bernards, R. (2021). Identification of Autophagy-Related Genes as Targets for Senescence Induction Using a Customizable CRISPR-Based Suicide Switch Screen. Mol. Cancer Res. *19*, 1613–1621. https://doi.org/10.1158/1541-7786.MCR-21-0146.
16. Dias, M.H., Friskes, A., Wang, S., Neto, J.M.F., Gemert, F.v., Mourragui, S., Kuiken, H.J., Mainardi, S., Alvarez-Villanueva, D., Lieftink, C., et al. (2023). Paradoxical activation of oncogenic signaling as a cancer treatment strategyPrepaint at. bioRxiv. https://doi.org/10.1101/2023.02.06.527335.
17. Hangauer, M.J., Viswanathan, V.S., Ryan, M.J., Bole, D., Eaton, J.K., Matov, A., Galeas, J., Dhruv, H.D., Berens, M.E., Schreiber, S.L., et al. (2017). Drug-tolerant persister cancer cells are vulnerable to GPX4 inhibition. Nature *551*, 247–250. https://doi.org/10.1038/nature24297.
18. Wang, L., Jin, H., Jochems, F., Wang, S., Lieftink, C., Martinez, I.M., De Conti, G., Edwards, F., de Oliveira, R.L., Schepers, A., et al. (2022). cFLIP suppression and DR5 activation sensitize senescent cancer cells to senolysis. Nat. Cancer *3*, 1284–1299. https://doi.org/10.1038/s43018-022-00462-2.
19. Dhimolea, E., de Matos Simoes, R., Kansara, D., Al'Khafaji, A., Bouyssou, J., Weng, X., Sharma, S., Raja, J., Awate, P., Shirasaki, R., et al. (2021). An Embryonic Diapause-like Adaptation with Suppressed Myc Activity Enables Tumor Treatment Persistence. Cancer Cell *39*, 240–256.e11. https://doi.org/10.1016/j.ccell.2020.12.002.
20. Delmore, J.E., Issa, G.C., Lemieux, M.E., Rahl, P.B., Shi, J., Jacobs, H.M., Kastritis, E., Gilpatrick, T., Paranal, R.M., Qi, J., et al. (2011). BET bromodomain inhibition as a therapeutic strategy to target c-Myc. Cell *146*, 904–917. https://doi.org/10.1016/j.cell.2011.08.017.
21. Lovén, J., Hoke, H.A., Lin, C.Y., Lau, A., Orlando, D.A., Vakoc, C.R., Bradner, J.E., Lee, T.I., and Young, R.A. (2013). Selective inhibition of tumor oncogenes by disruption of super-enhancers. Cell *153*, 320–334. https://doi.org/10.1016/j.cell.2013.03.036.
22. Shen, S., Faouzi, S., Bastide, A., Martineau, S., Malka-Mahieu, H., Fu, Y., Sun, X., Mateus, C., Routier, E., Roy, S., et al. (2019). An epitranscriptomic mechanism underlies selective mRNA translation remodelling in melanoma persister cells. Nat. Commun. *10*, 5713. https://doi.org/10.1038/s41467-019-13360-6.
23. Karki, P., Angardi, V., Mier, J.C., and Orman, M.A. (2021). A Transient Metabolic State in Melanoma Persister Cells Mediated by Chemotherapeutic Treatments. Front. Mol. Biosci. *8*, 780192. https://doi.org/10.3389/fmolb.2021.780192.
24. Zhang, Z., Tan, Y., Huang, C., and Wei, X. (2023). Redox signaling in drug-tolerant persister cells as an emerging therapeutic target. EBioMedicine *89*, 104483. https://doi.org/10.1016/j.ebiom.2023.104483.
25. Kuang, F., Liu, J., Xie, Y., Tang, D., and Kang, R. (2021). MGST1 is a redox-sensitive repressor of ferroptosis in pancreatic cancer cells. Cell Chem. Biol. *28*, 765–775.e5. https://doi.org/10.1016/j.chembiol.2021.01.006.
26. Raha, D., Wilson, T.R., Peng, J., Peterson, D., Yue, P., Evangelista, M., Wilson, C., Merchant, M., and Settleman, J. (2014). The cancer stem cell marker aldehyde dehydrogenase is required to maintain a drug-tolerant tumor cell subpopulation. Cancer Res. *74*, 3579–3590. https://doi.org/10.1158/0008-5472.CAN-13-3456.
27. Zhao, J., Jia, Y., Mahmut, D., Deik, A.A., Jeanfavre, S., Clish, C.B., and Sankaran, V.G. (2023). Human hematopoietic stem cell vulnerability to ferroptosis. Cell *186*, 732–747.e16. https://doi.org/10.1016/j.cell.2023.01.020.
28. Kim, R., Hashimoto, A., Markosyan, N., Tyurin, V.A., Tyurina, Y.Y., Kar, G., Fu, S., Sehgal, M., Garcia-Gerique, L., Kossenkov, A., et al. (2022). Ferroptosis of tumour neutrophils causes immune suppression in cancer. Nature *612*, 338–346. https://doi.org/10.1038/s41586-022-05443-0.
29. Wang, L., Lankhorst, L., and Bernards, R. (2022). Exploiting senescence for the treatment of cancer. Nat. Rev. Cancer *22*, 340–355. https://doi.org/10.1038/s41568-022-00450-9.
30. Patel, S.A., and Minn, A.J. (2018). Combination Cancer Therapy with Immune Checkpoint Blockade: Mechanisms and Strategies. Immunity *48*, 417–433. https://doi.org/10.1016/j.immuni.2018.03.007.
31. Jochems, F., Thijssen, B., De Conti, G., Jansen, R., Pogacar, Z., Groot, K., Wang, L., Schepers, A., Wang, C., Jin, H., et al. (2021). The Cancer SENESCopedia: A delineation of cancer cell senescence. Cell Rep. *36*, 109441. https://doi.org/10.1016/j.celrep.2021.109441.
32. Hao, Y., Hao, S., Andersen-Nissen, E., Mauck, W.M., 3rd, Zheng, S., Butler, A., Lee, M.J., Wilk, A.J., Darby, C., Zager, M., et al. (2021). Integrated analysis of multimodal single-cell data. Cell *184*, 3573–3587.e29. https://doi.org/10.1016/j.cell.2021.04.048.
33. Kinker, G.S., Greenwald, A.C., Tal, R., Orlova, Z., Cuoco, M.S., McFarland, J.M., Warren, A., Rodman, C., Roth, J.A., Bender, S.A., et al. (2020). Pan-cancer single-cell RNA-seq identifies recurring programs of cellular heterogeneity. Nat. Genet. *52*, 1208–1218. https://doi.org/10.1038/s41588-020-00726-6.
34. Barkley, D., Moncada, R., Pour, M., Liberman, D.A., Dryg, I., Werba, G., Wang, W., Baron, M., Rao, A., Xia, B., et al. (2022). Cancer cell states recur across tumor types and form specific interactions with the tumor microenvironment. Nat. Genet. *54*, 1192–1201. https://doi.org/10.1038/s41588-022-01141-9.

STAR★METHODS

KEY RESOURCES TABLE

REAGENT or RESOURCE	SOURCE	IDENTIFIER
Antibodies		
Rabbit polyclonal anti-BRD2 antibody	Bethyl	Cat# A302-582A; RRID: AB_2034828
Cas9 (7A9-3A3) antibody	Cell Signaling Technology	Cat# 14697, RRID: AB_2750916
β-Actin (8H10D10) Mouse mAb antibody	Cell Signaling Technology	Cat# 3700, RRID: AB_2242334
Goat Anti-Rabbit IgG (H L)-HRP Conjugate antibody	Bio-Rad	Cat# 170–6515, RRID: AB_11125142
Goat Anti-Mouse IgG (H L)-HRP Conjugate antibody	Bio-Rad	Cat# 170–6516, RRID: AB_11125547
Chemicals, peptides, and recombinant proteins		
DMEM High Glucose, pyruvate	Gibco	Cat# 41966-029
RPMI 1640 medium	Gibco	Cat# 21875-034
Penicillin-Streptomycin	Gibco	Cat# 15140-122
Trypsin-EDTA (0.05%), phenol red	Gibco	Cat# 25300-054
L-Glutamine 200mM	Gibco	Cat# 25030-024
Matrigel Basement Membrane Matirx	Corning	Cat# 354234
Polybrene	Santa Cruz Biotechnology	Cat# sc-134220
Polyethylenimine hydrochloride	Sigma-Aldrich	Cat# 764892
Doxycycline hyclate	Sigma-Aldrich	Cat# D5207
N-acetylcysteine amide	Sigma-Aldrich	Cat# A0737
Gefitinib	Selleck	Cat# S1025
Osimertinib	Selleck	Cat# S7297
Alisertib	Selleck	Cat# S1133
Crizotinib	Selleck	Cat# S1068
Sotorasib (AMG510)	Selleck	Cat# S8830
Ferrostatin-1	Selleck	Cat# S7243
Z-VAD-FMK	Selleck	Cat# S7023
B/B Homodimerizer	Takara	Cat# 635069
Trametinib	MedKoo	Cat# 201458
Dabrafinib	MedChemExpress	Cat# HY-14660
RSL3	Selleck	S8155
*NEO*2734	Selleck	S9648
ARV-771	Selleck	S8532
CC90010	Selleck	S3573
ABT263	Selleck	S1001
Critical commercial assays		
ISOLATE II PCR and Gel Kit	Meridian Bioscience	Cat# BIO-52060
Auick-DNA Miniprep Kit	ZYMO Research	Cat# D3024&D3025
SensiFAST cDNA Synthesis Kit	Meridian Bioscience	Cat# BIO-65054
SensiFAST SYBR Lo-ROX Kit	Meridian Bioscience	Cat# BIO-94020
Deposited data		
scRNA seq data	Zenodo	https://doi.org/10.5281/zenodo.10575819
Bulk RNA-seq data	Zenodo	https://doi.org/10.5281/zenodo.10575970
Experimental models: Cell lines		
PC-9; human EGFR-mutant NSCLC, male	ATCC	STR profiled
H358; human G12C-mutant NSCLC, male	ATCC	CRL-5807
GTL-16: human MET amplified gastric adenocarcinoma	VictoriaWANG Lab	N/A

(*Continued on next page*)

Continued

REAGENT or RESOURCE	SOURCE	IDENTIFIER
A375: human BRAF mutant melanoma, femal	ATCC	CRL-1619
HEK293	ATCC	CRL-1573
Experimental models: Organisms/Strains		
Mouse: Ncr nude mice	Janvier Laboratories	N/A
Oligonucleotides		
qPCR primers, see Table S3	IDT	N/A
shRNA targeting sequence, see Table S3	TRC library	N/A
Recombinant DNA		
MISSION® TRC-Hs 1.0 (Human)	Sigma-Aldrich	N/A
lentiGuide -Puro	Addgene	Cat# 52963
Human Brunello kinome pooled library, guides 1–4 in lentiGuide-Puro backbone	Addgene	Cat# 75312
hORFeome V8.1 Library	Broad	N/A
Software and algorithms		
Graphpad Prism		https://www.graphpad.com/features
Single Cell 3′ v3 with cellranger-7.0.1		https://support.10xgenomics.com/
R version 4.2.3		https://www.R-project.org/
Seurat v 4.3.0		http://satijalab.org/seurat/
Other		
Key codes for scRNA analyses	Zenodo	https://doi.org/10.5281/zenodo.10679694

RESOURCE AVAILABILITY

Lead contact

Further information and requests for resources and reagents should be directed to René Bernards (r.bernards@nki.nl).

Materials availability

All unique/stable reagents generated in this study are available from the lead contact with a completed Materials Transfer Agreement.

Data and code availability

Sequencing data generated in this study has been deposited at Zenodo through https://doi.org/10.5281/zenodo.10575819 and https://doi.org/10.5281/zenodo.10575970 for scRNA-seq and bulk RNA-seq accordingly. Key codes are available at https://github.com/YangJAT/DTP and https://doi.org/10.5281/zenodo.10679694. This paper does not report original code. Any additional information required to reanalyze the data reported in this paper is available from the lead contact upon reasonable request.

EXPERIMENTAL MODEL AND STUDY PARTICIPANT DETAILS

Animal models

Male/Female Balb/c nude (cAnN/Rj), 6-week old, were purchased from Janvier Laboratories, The Netherlands. PC9 cells (5 million per mice) were injected into the right flanks of nude female mice. Tumor volume was determined by a digital caliper and quantified by the modified ellipsoidal formula (tumor volume = 1/2(length × width2)). Tumor volume and mice weight were monitored three times a week. Osimertinib (10 mg/kg once daily) and *NEO*2734 (4 mg/kg, 5 days/week) were administered orally as a suspension using 0.5% hydroxypropyl methylcellulose (HPMC) or 10% DMSO+20%Cremophor EL+70% Saline as vehicle, respectively. Control vehicle mice received 0.5% HPMC and 10% DMSO+20%Cremophor EL+70% Saline administered orally. When the tumors reached approximately 200mm3 of volume, mice were randomly assigned into various treatment groups with 6 mice per group. For the sequential study, mice were randomized to receive either vehicle, 4 mg/kg *NEO*2734, 10 mg/kg Osimertinib for 28 days switched to either Vehicle-NEO2734 or 4 mg/kg *NEO*2734. For the upfronted combinational treatment, mice were randomized to receive either Osimertinib or Osimertinib and *NEO*2734 for 28 days. After that, the treatment will be suspended. For A375 xenograft study, 5 million cells were injected into the right flanks of nude mice. Dabrafenib (Dabra) and Trametinib (Trame) were dissolved in 10% DMSO+20% Cremophor EL+70% Saline and injected by oral gavage. When the tumors reached approximately 200mm3 of volume, mice were randomized to receive either vehicle, 4 mg/kg *NEO*2734, 30 mg/kg Dabra+0.6 mg/kg Trame for 28 days switched to either

Vehicle-NEO2734 or 4 mg/kg *NEO*2734, combinational treatment of Dabra+Trame, triple treatment of Dabra+Trame+*NEO*2734. The mice were maintained and monitored for tumors relapse and humanely euthanized at endpoint.

All *in vivo* studies were conducted at the Netherlands Cancer Institute with the approval of the Institutional guidelines.

Cell line authentication

Cell lines PC9, H358 and GTL-16 were grown in RPMI-1640 (Gibco), supplemented with 10%FBS, and 1% penicillin/streptomycin (Gibco) and 1% glutamine (Gibco). A375 and HEK293 cells were grown in DMEM supplemented with 10%FBS, and 1% penicillin/streptomycin (Gibco) and 1% glutamine (Gibco). Cell lines PC9, A375 (CRL-1619), H358 (CRL-5807) and HEK293 (CRL-1573) were purchased from ATCC. GTL-16 was a gift from Victoria Wang. All cell lines have been validated by STR profiling and were regularly tested for mycoplasma spp with a PCR-based assay.

METHOD DETAILS

Reagents

DMEM High Glucose (Gibco), RPMI 1640 (Gibco), Trypsin 0.05% (Gibco), penicillin/streptomycin 1X (Gibco), Glutamine (Gibco), Matrigel (Corning), Polybrene (Santa Cruz Biotechnology), Polyethylenimine (Sigma-Aldrich), BRD2 antibody (Bethyl Laboratories), β-actin (Cell Signaling Technology), Osimertinib (MedchemExpress, Selleck), CID compound (Takara 635088), Doxycycline (Sigma), Alisertib (Selleck), Trametinib (Medko), Dabrafenib (MedchemExpress), Crizotinib (Selleck), AMG510 (Selleck), RSL3(Selleck), *NEO*2734(Selleck), ARV-771(Selleck), CC90010 (Selleck), ABT-263 (Selleck), Ferrostatin (Selleck), Z-VAD-FMK (Selleck), N-acetylcysteine amide (Sigma).

Drug treatments

Conditions for DTP induction are listed as follows: For PC9, cells were treated with either 200nM Osimertinib or 500nM Gefitinib for 1 week followed by Osi/Gefi plus 10nM CID for 1 week; A375 cells were treated with 2μM Dabrafenib plus 2 μM Trametinib. GTL-16 cells were treated with 2μM Crizotinib; H358 were treated with 2μM AMG510. Treatment time were 2 weeks for DTP induction. Cells were treated with 1 μg/ml doxycycline for Cas9 induction. For the rescue experiments, DTPs were treated with BET inhibitors together with either ferrostatin at 2.5μM, NAC at 2.5 mM and Z-VAD-FMK at 10μm. Concentrations of BET inhibitors and RSL3 were 0.25μM for *NEO*2734, 0.25 μM for ARV-771, 0.25μM for CC90010, 1 μM for RSL3 and 125 ng/ml for Conatumumab.

Compound screen

Workflow for compound screen was summarized in Figure 1A. Cells were screened for sensitivity against a panel of 163 small-molecule inhibitors from a stress-focused compound library (Matheus, Dias et al., 2023). In brief, PC9 cells were treated with 2.5 μM Alisertib for 7 days for senescence induction, gefitinib plus CID for 2 weeks for DTP induction. Then parental proliferating cells, senescent cells, DTPs and DTEPs were seeded in 384-well plates. All compounds were tested at fifteen concentrations. Each plate included 8 wells containing DMSO (as a negative control) and 8 wells containing 10 μM PAO (as a positive control). The cell viability in each well was determined using CellTiter-Blue reagent (Promega). AUC scores were calculated for each compound. The relative sensitivities of parental PC9-SS, senescent cells, DTPs and DTEPs were normalized against parental conditions after subtraction of background signal.

CRISPR/Cas9-based genetic screen

Workflow for CRISPR based genetic screen was summarized in Figure 1C. To ensure cells to be homogenously induced into DTPs while maintain high genome editing capacity, monoclonal cells with high CAS9 induction by doxycycline were selected. Gene editing efficiency was tested after DTP induction. The cells were infected with lentiviral vector pXPR-011 containing EGFP with gRNA against EGFR first and then were induced into DTPs. Gene editing efficiency was determined by the percentage of EGFP positive cells after 10 days of doxycycline treatment (Figures S2A–S2C). For the genetic screen in Figure 1C, monoclonal PC9-iCas9 cells were infected with kinome-wide gRNA virus with 500 coverage and multiplicity of infection of 0.3. After puromycin selection, these cells were seeded for DTP induction as described above. Afterward, DTPs were reseeded and switched to doxycycline treatment for 10days. Changes in gRNAs representation after 10days of dox induction were determined by Illumina deep sequencing. Parental proliferating cells were included as the control arm to filter out essential genes and to determine the sgRNAs specifically dropped out in DTP arm.

RNA-sequencing and GSEA analysis

Cells were seeded in 150-mm cell culture dishes and were treated with different stand of care therapy (See Drug treatment-DTP induction). Paired samples of PAR/DTP were collected for RNA seq at T0. DTPs were seeded into 6 well plate one day before *NEO*2374 treatment. Samples were collected 48h and 72h after treatment. RNA isolation, library preparation and RNA sequencing were performed as described before.[31] RNA-seq data for the samples was normalized based on a relative total size factor. Data was then filtered for protein coding genes and in case of more than one transcript for a gene, the mean was taken. For dtp versus parental, both at timepoint 0, the log2 fold change was calculated. For DTEP-UN versus DTEP-TR, both at time point 1 and time point 2,

the log2 fold change wea calculated. A list was created with the genes sorted on this log2 fold change value in decreasing order. GSEA was performed based on this list for both the MsigDb Hallmark genesets and the KEGG genesets using the bioconductor package fgsea (Gennady Korotkevich et al. 2021). The clustering heatmaps were created using the heatmap.2 function of the R-package gplots. The difference of persisters derived from different tissue origins was reflected by difference among NES score (indicates c in the formula) calculated through GSEA analysis for paired DTP T0 vs. Par T0. Formula used for calculation is listed below:

$$distance(sample\ 1; sample\ 2) = \frac{\sum_{i=1}^{n} |c_i^1 - c_i^2|}{n}$$

where n is the total number of characteristics, c_i^1 and c_i^2 are respectively the i-th characteristics of the sample 1 and 2.

Single cell RNA sequencing

For each single cell suspension (Parental PC9, DTPs, DTEPs-UN-T1, DTEPs-TR-T1, DTEP-UN-T2, DTEP-TR-T2), approximately 5000 cells were loaded per sample. Sample preparations and library constructions were performed according to 10x Genomics manufacturer's instructions. The data processing (normalization, dimensional reduction, clustering and visualization) was done in R version 4.2.3(https://www.R-project.org/.) using Seurat v 4.3.0.[32] Gene marker identification was also performed using Seurat v 4.3.0 using the Wilcox rank-sum test. The differential expression were performed on scaled data. Uniform Manifold Approximation and Projection (UMAP) reduction and the FindNeighbors were performed using first 30 PCA components as recommended in the Seurat SCT processing vignette. Signature scores for each cell were calculated using the AddModuleScore function, and the senescence-related gene lists were achieved from previous publications.[33,34] DTEP-UN-T1 and DTEP-UN-T2, DTEP-TR-T1 and DTEP-TR-T2 were analyzed as duplicates.

Plasmids

shRNA vectors were collected from the TRC library (Table S3). cFlip overexpression lentiviral vectors were collected from the BROAD ORF cDNA library. gRNA cloning vector pLentiGuide-puro (52963) and human CRIPSR Knockout Pooled Library (Kinome) (75312) were purchased from Addgene. The edit-R inducible Lentiviral Cas9 vector (NC1606271) was purchase from Dharmacon.

Cell viability measurement

Cell viability was detected by CellTiter-Blue Cell Viability Assay kit (G8081, Promega) according to the manufacturers' instructions. DTPs were induced by different stand of care therapy for 14 days. Next, parental and DTP cells were trypsinized, washed out the primary treatment and seeded at an equal cell density in the plates. Afterward, cells were treated with other drugs. CellTiter-Blue reagent was added at day 5 and measurement was performed by EnVision multi-label plate reader (PerkinElmer). For the rescue experiments, cells were treated with BET inhibitors/RSL3 together with NAC/Ferrostatin/Z-VAD-FMK with the dose indicated in figure legend for 5 days followed by replenished with fresh medium for another 7 days. Afterward, cellTiter-Blue reagent was added and measurement was performed. Dose-response curves were calculated by PRISM. Triplicate were performed for each group.

Long term colony formation assays

Parental proliferating cells and DTPs were seeded into 96 well plates at 2,000 cells/well. The next day, cells were treated with drugs. Parental proliferating cells were collected at day 5. DTEPs were collected at day 10 to let the control groups reach over 90% of confluence. At the end of the assay, cells were fixed with 3.7% formaldehyde (1.04002, Millipore) diluted in PBS, stained with 2% crystal violet overnight (HT90132 Sigma-Aldrich). Images were scanned with Fiji. Triplicate were performed for each group.

Incucyte cell proliferation assays and caspase-3/7 activity monitoring

Cells were seeded in 96 well plates (2,000 cells per well in 100μL of growth medium). The next day, drugs were added onto cells as indicated. Apoptosis marker staining was performed by adding CellEvent caspase-3/7 green apoptosis assay reagent (Molecular Probes) at 1,000 times dilution to each well. The cells were subsequently scanned every 6 h using the Incucyte ZOOM live cell analysis system (Essen Bioscience) typically for a total of 72 h. Cell confluence and GFP signal were measured and quantified by the incucyte imaging system. Triplicate were performed for each group.

Lentiviral transductions

Lentiviral particles were created using lentivirus packaging system containing pCMV-VSV-G (Addgene 8454), pRSV-Rev (Addgene 12253), and pMDLg/pRRE (Addgene 12251). Lentiviral supernatants were collected after transfection performed in HEK293 cells. Lentivirus transduced cells were selected with 2 μg/ml puromycin or 10 μg/ml blasticidin.

CRISPR mediated knockout of BRD2

BRD2 knockout cells were generated by using the gRNA (5′- CCTGAGATACCTACCACTGT-3′). gRNA was cloned into LentiGuide-ouro (Addgene plasmid 52963) via BsmBI sites with Gibson Assembly Master Mix (E2611, NEB). Afterward, gRNA-BRD2 were

transduced into PC9-iCas9 cells by lentiviral infection. After puromycin selection, doxycycline was added to activate genome editing. After 72h, $BRD2^{KO}$ clones were picked.

Western Blotting and antibodies

Cells were seeded in the culture medium and lysed in RIPA buffer supplemented with protease inhibitors (Roche) and phosphatase inhibitors cocktails II and III (Sigma). Twenty micrograms of total protein were used for immunoblotting according to the antibody manufacture's recommendations. Samples were processed with Novex NuPAGE Gel Electrophoresis Systems (Invitrogen).

RNA extraction and quantitative PCR (QPCR)

Total RNA was extracted using Quick-RNA MiniProp (R1055, Zymo Research). The RNA concentrations were measured with Nanodrop (Thermo Fisher Scientific) and 1μg of total RNA was used for cDNA cDNA synthesis using Maxima Universal FirstStrand cDNA synthesis kit (Thermo Fisher Scientific). The QPCR reactions were set up using FastStart Universal SYBP Green master (Rox) from Roche. The experiments were performed according to the manufacturers' instructions. All reactions were run in triplicate. Primer information can be found in Table S3.

Senescence-associated β-galactosidase staining

PC9 parental and DTP cells were plated into 6-well plates at 100,000 cells/well in triplicate. β-galactosidase activity was stained one day after with β-galactosidase Staining kit (Sigma) according to manufacturer's protocol. After staining, cells were imaged (3 images/well), and stained cells were manually counted from the images.

Reactive oxygen species staining and flow cytometry

Parental and DTPs were seeded into 6 well plates at 100,000 cells/well. DTPs were maintained in either fresh medium to obtain DTEPs or in drug containing medium to maintain DTP status. The next day, DTEPs were treated with *NEO*2734 or DMSO at dose of 0.5 μM for 72h. Intracellular ROS levels were determined by CellROX Green Flow Cytometry Assay Kit (Life Technologies) according to kit protocol. After staining, cells were measured by flow cytometry on a BD LSRFortessa and analyzed by Flowjo v.10.

QUANTIFICATION AND STATISTICAL ANALYSIS

Statistical analyses

Two-tailed unpaired t-test with Welch's correction were applied to compare statistical significance between two groups. All statistical analyses were generated using GraphPad Prism 9 software, except for bulk RNA seq and scRNA seq analysis where statistical analyses were run in R. Data are presented as mean ± standard deviation or standard error, as indicated in the figure legends. A P-value less than 0.05 was considered statistically significant in all analyses ($P < 0.05$: *; $P < 0.01$: **; $P < 0.001$: ***). Any cutoffs used for P-value or FDR are indicated in the figure legends. All analyses were performed with 3–6 replicates as indicated in the method details. In animal experiments n represents the number of animals in treatment groups.

Cell Reports Medicine, Volume *5*

Supplemental information

Targeting of vulnerabilities of drug-tolerant persisters identified through functional genetics delays tumor relapse

Mengnuo Chen, Sara Mainardi, Cor Lieftink, Arno Velds, Iris de Rink, Chen Yang, Hendrik J. Kuiken, Ben Morris, Finn Edwards, Fleur Jochems, Olaf van Tellingen, Manon Boeije, Natalie Proost, Robin A. Jansen, Shifan Qin, Haojie Jin, J.C. Koen van der Mijn, Arnout Schepers, Subramanian Venkatesan, Wenxin Qin, Roderick L. Beijersbergen, Liqin Wang, and René Bernards

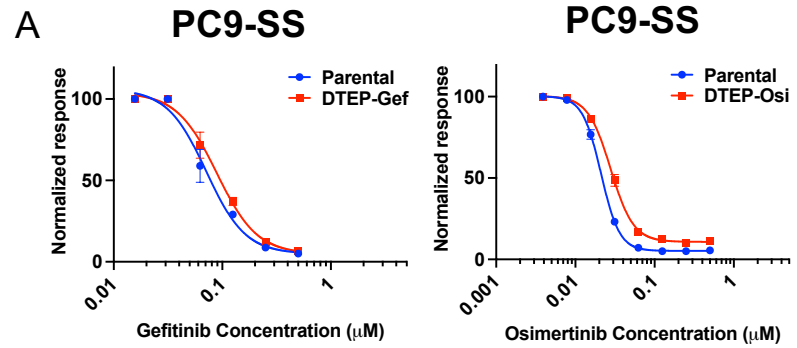

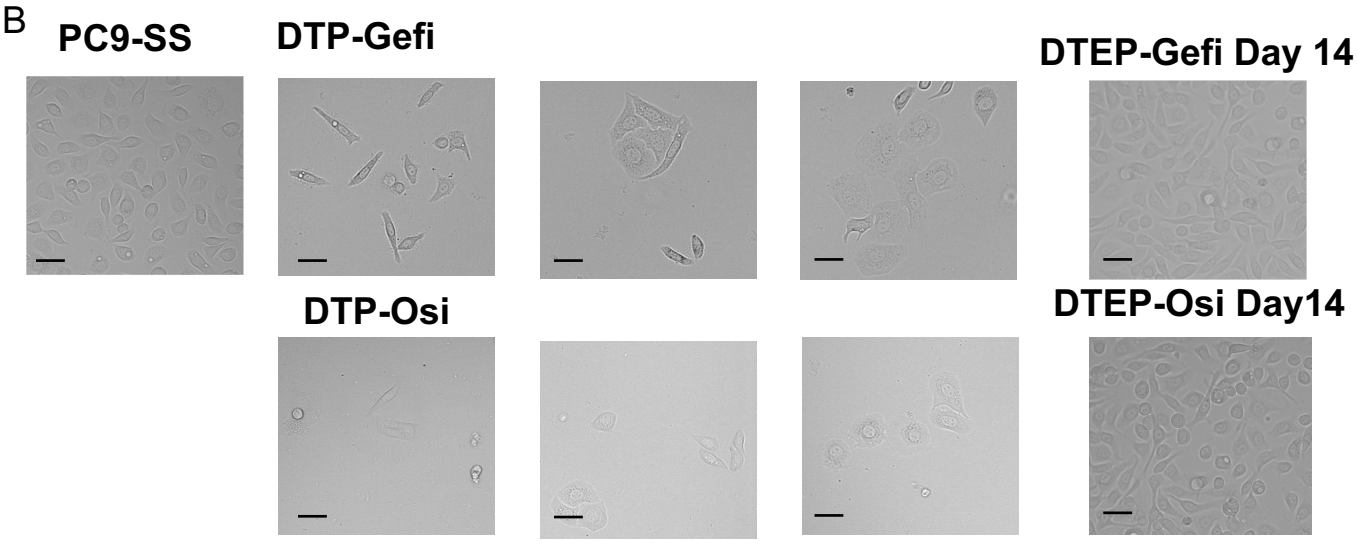

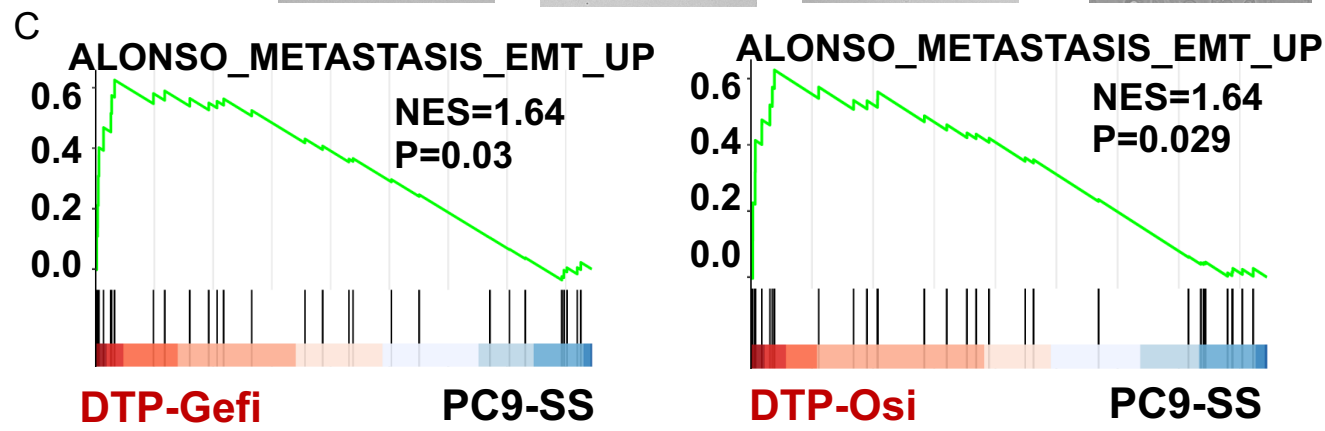

D

IC50	PC9-SS Gefitinib	PC9-SS Osimertinib	GTL-16 Crizotinib	A375 Dabra+Trame	H358 AMG510
Parental	71.23nM	21.08nM	117.4nM	11.49nM	16.42nM
DTEP	89.18nM	27.90nM	193.3nM	12.227nM	16.42nM

Figure S1. Persisters induction and purificaition in PC9, A375, GTL16 and H358. Related to Figures 1 and 2. (A) Five-day dose-response curve of DTPs and DTEPs to corresponding EGFR inhibitors. Error bars represent mean ± s.d., n = 3 independent experiments. Statistical significance was calculated by two-tailed Student's t-test. (B) Representative images of morphologies for Parental, DTP and DTEPs in PC9. Black scale bars, 50 μm. (C) GSEA analysis for EMT signature enrichment in DTPs in comparison with parental PC9 cells. (D) IC50 values to standard of care therapy in paired parental and DTEPs derived from PC9, GTL-16, A375 and H358. Days for culturing after drug wash out were 21, 30 and 14 for DTEPs derived from GTL-16, A375 and H358 accordingly. IC50, half-maximum inhibitory concentration.

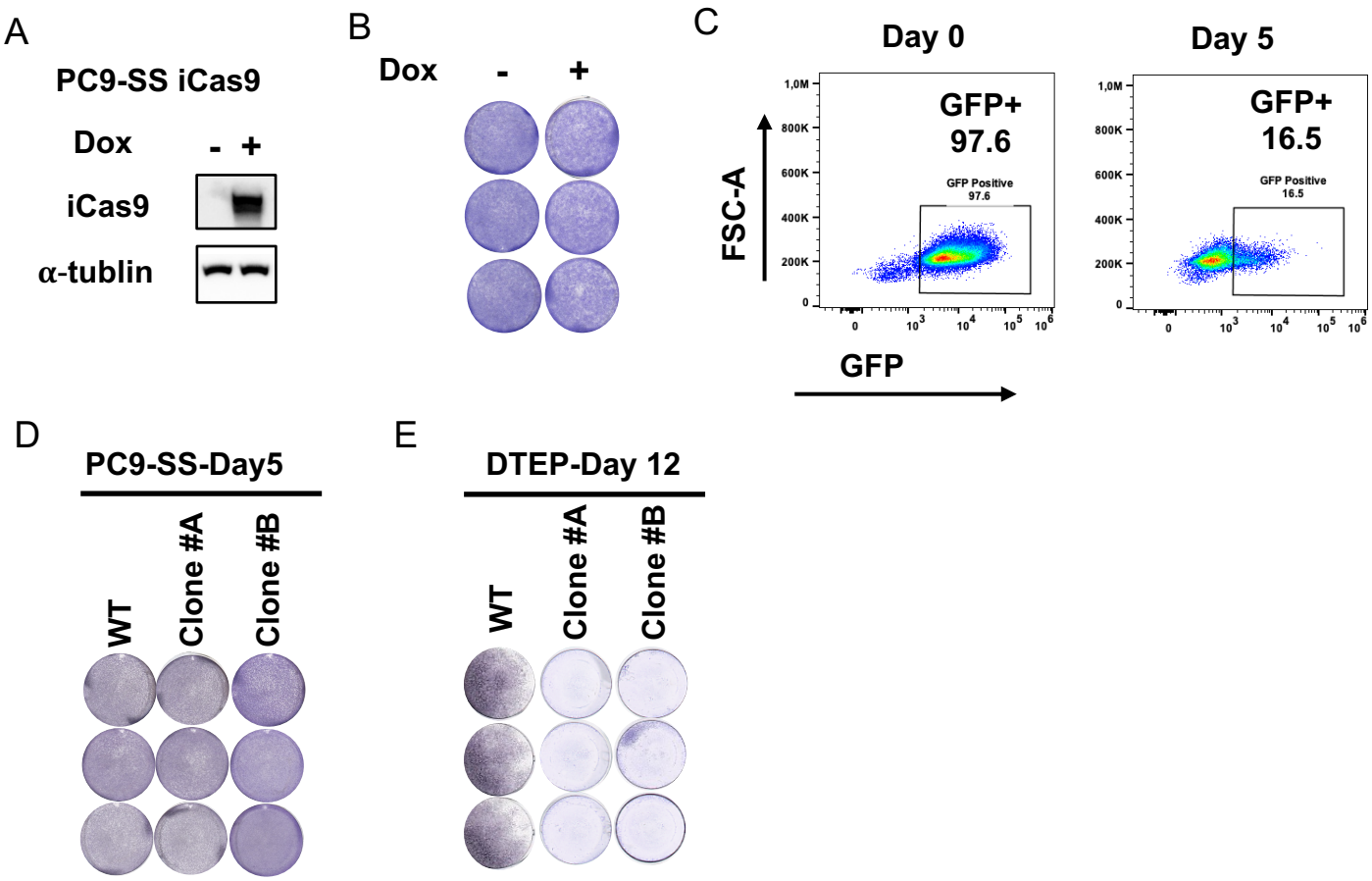

Figure S2. BRD2 knockout abolished the outgrowth of DTPs into DTEPs while had miner effect on proliferation of parental PC9 cells. Related to Figure 1.(A) Western blot detection of Cas9 expression after 24h Dox(doxycycline) treatment (1μg ml^{-1}). (B) Colony formation assay for PC9-SS iCas9 cells after 5 days Dox treatment (1μg ml^{-1}). Replicates were performed for each group. (C) Editing efficiency detection reflected by percentage of GFP positive cells after 10 days Dox treatment (1μg ml^{-1}). (D) Colony formation for WT and BRD2 knockout clones of PC9. Collected at day 5. (E) Long-term colony formation for WT and BRD2 knockout DTEPs induced by Osimertinib. Collected at day 12. Replicates were performed for each group.

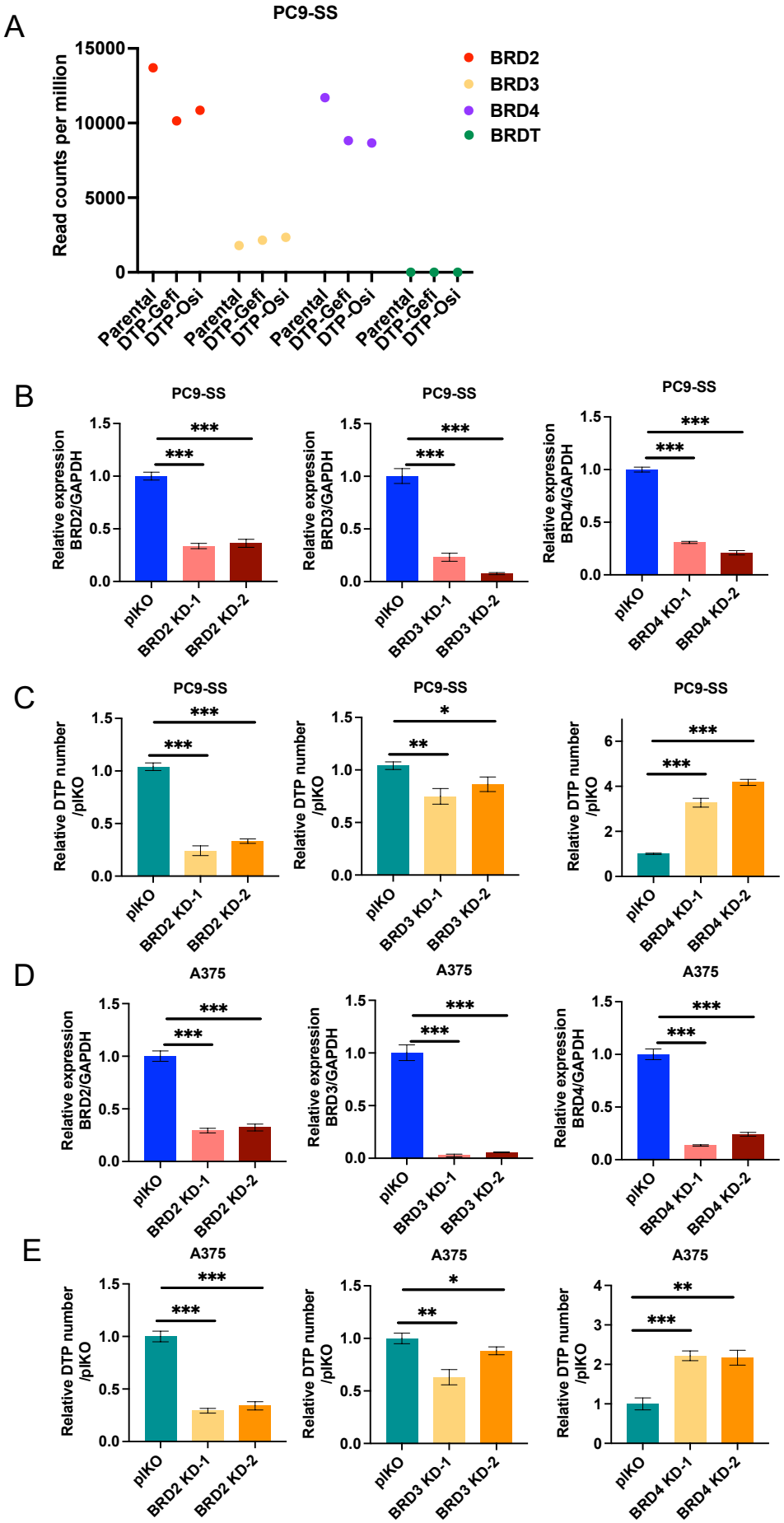

Supplementary Figure 3. DTP formation analysis in BRD2-4 knockdown cells in PC9 and A375. Related to Figures 1 and 2. (A) Read counts per million for BRD2-4 and BRDT in parental PC9, DTP-Gefi and DTP-Osi. (B) Knockdown efficiency of BRD2-4 by qRT-PCR in PC9. (C) DTP formation analysis in BRD2-4 knockdown groups as compared to plKO in PC9. (D) Knockdown efficiency of BRD2-4 by qRT-PCR in A375. (E) DTP formation analysis in BRD2-4 knockdown groups as compared to plKO in A375. Error bars in B-E represent mean ± s.d., n = 3 independent experiments. Statistical significance was calculated by two-tailed Student's t-test (*$P \leq 0.05$, ** $P \leq 0.01$, *** $P \leq 0.001$).

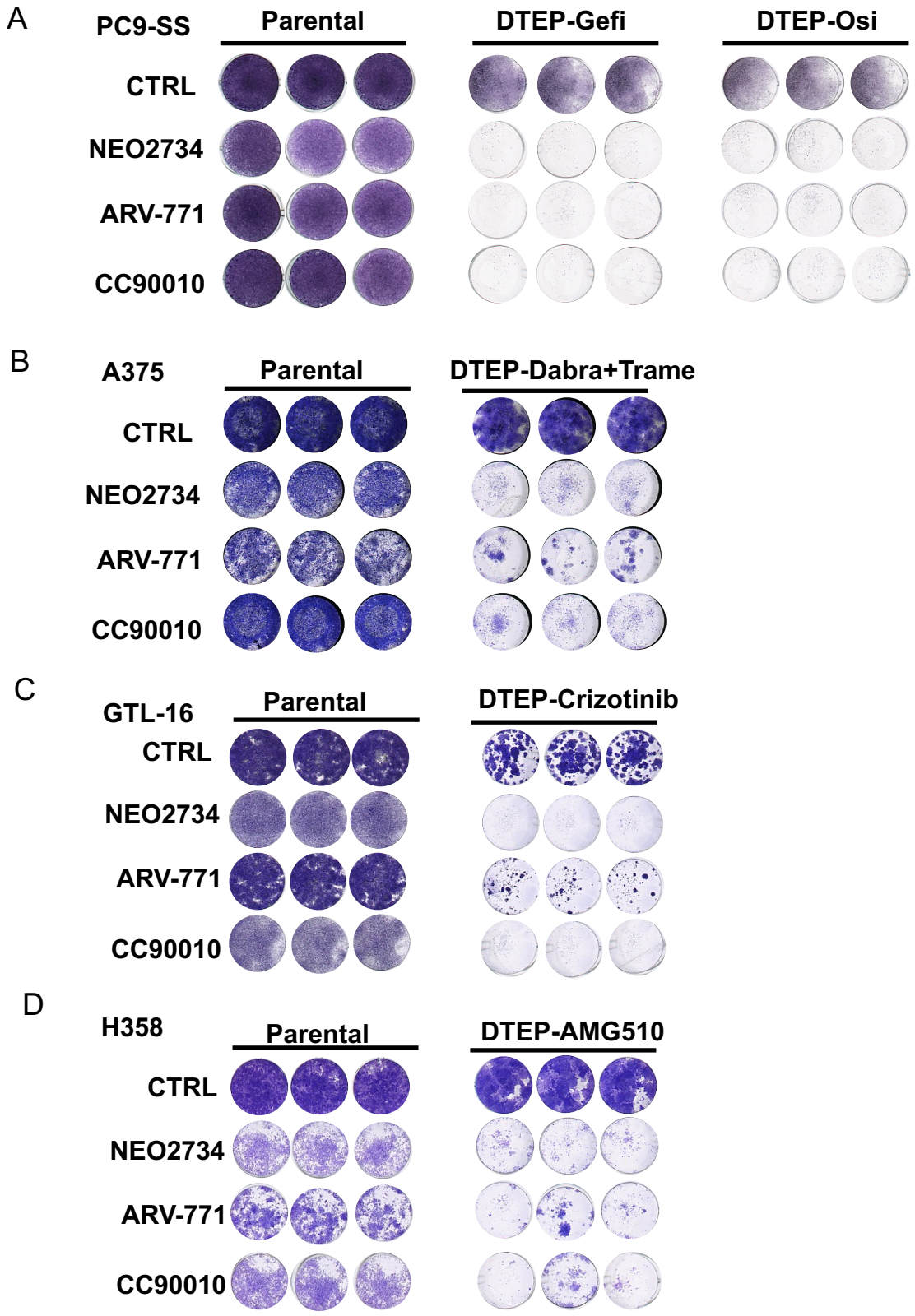

Figure S4. BET inhibitors suppress DTEPs validated by long-term colony formation assay. Related to Figures 1 and 2. (A-D) Long-term colony formation assay for paired parental and persisters from PC9, A375, GTL-16 and H358 treated with three BET inhibitors NEO2734, ARV-771 and CC90010. Parental were collected at Day 5. DTEPs were collected at day 12 except for GTL-16 collected at Day 21 (NEO2734: 0.08μM; ARV-771: 0.08μM; CC90010: 0.08μM). Replicates were performed for each group.

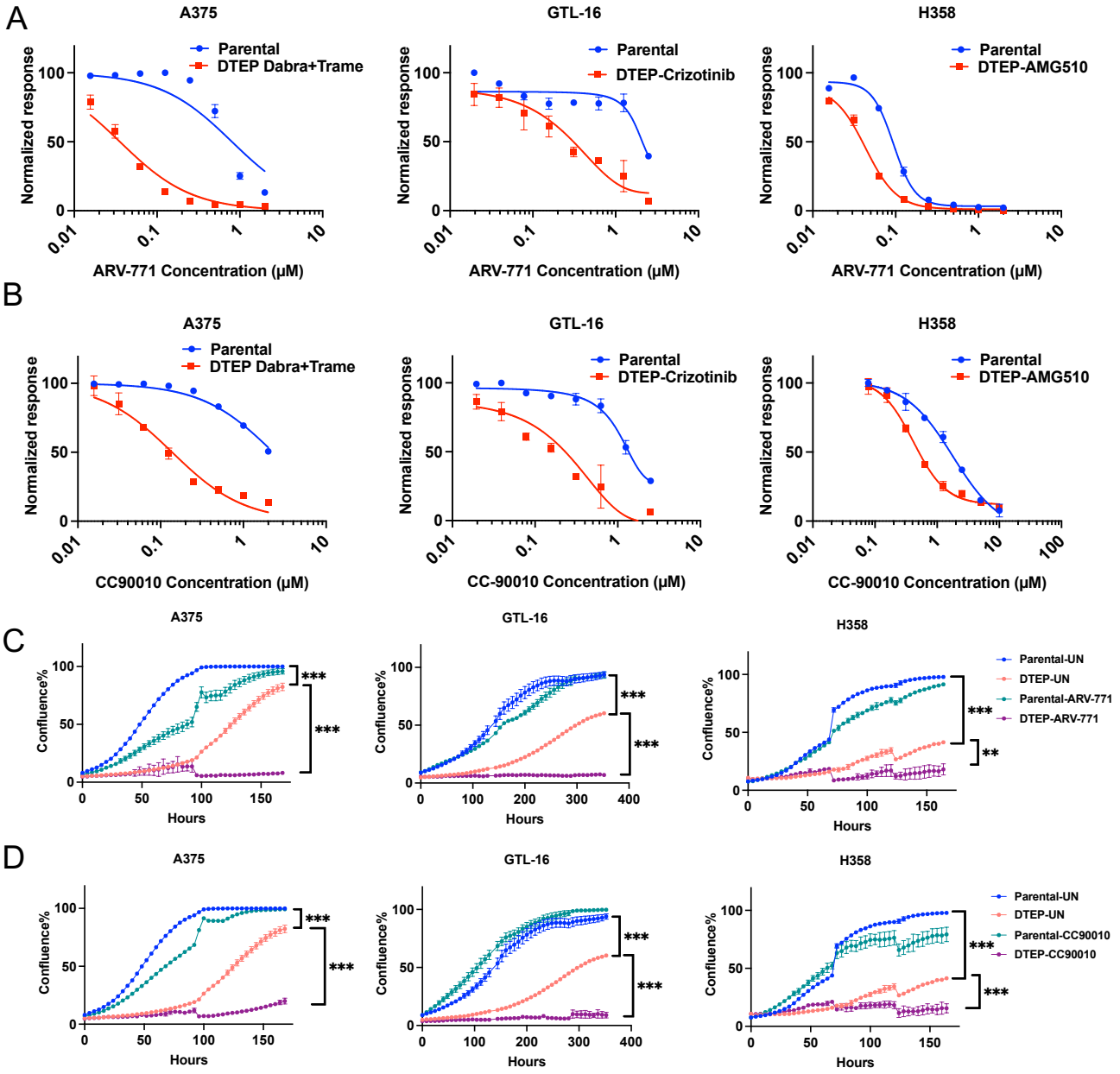

Figure S5. BET inhibitors suppress DTEPs validated by cell viability and incucyte growth monitoring. Related to Figure 2. (A) Five-day dose-response curve for paired parental and persisters from A375, GTL-16 and H358 to DMSO or BET inhibitor ARV-771. (B) Five-day dose-response curve for paired parental and persisters from A375, GTL-16 and H358 to DMSO or BET inhibitor CC90010. (C) Incucyte proliferation for paired parental and persisters from A375, GTL-16 and H358 treated with DMSO or ARV-771 (NEO2734: 0.08μM; ARV-771: 0.08μM; CC90010: 0.08μM). (D) Incucyte proliferation for paired parental and persisters from A375, GTL-16 and H358 treated with DMSO or CC90010 (NEO2734: 0.08μM; ARV-771: 0.08μM; CC90010: 0.08μM). Error bars in A-D represent mean ± s.d., n = 3 independent experiments. Statistical significance was calculated by two-tailed Student's t-test (*P ≤ 0.05, ** P ≤ 0.01, *** P ≤ 0.001).

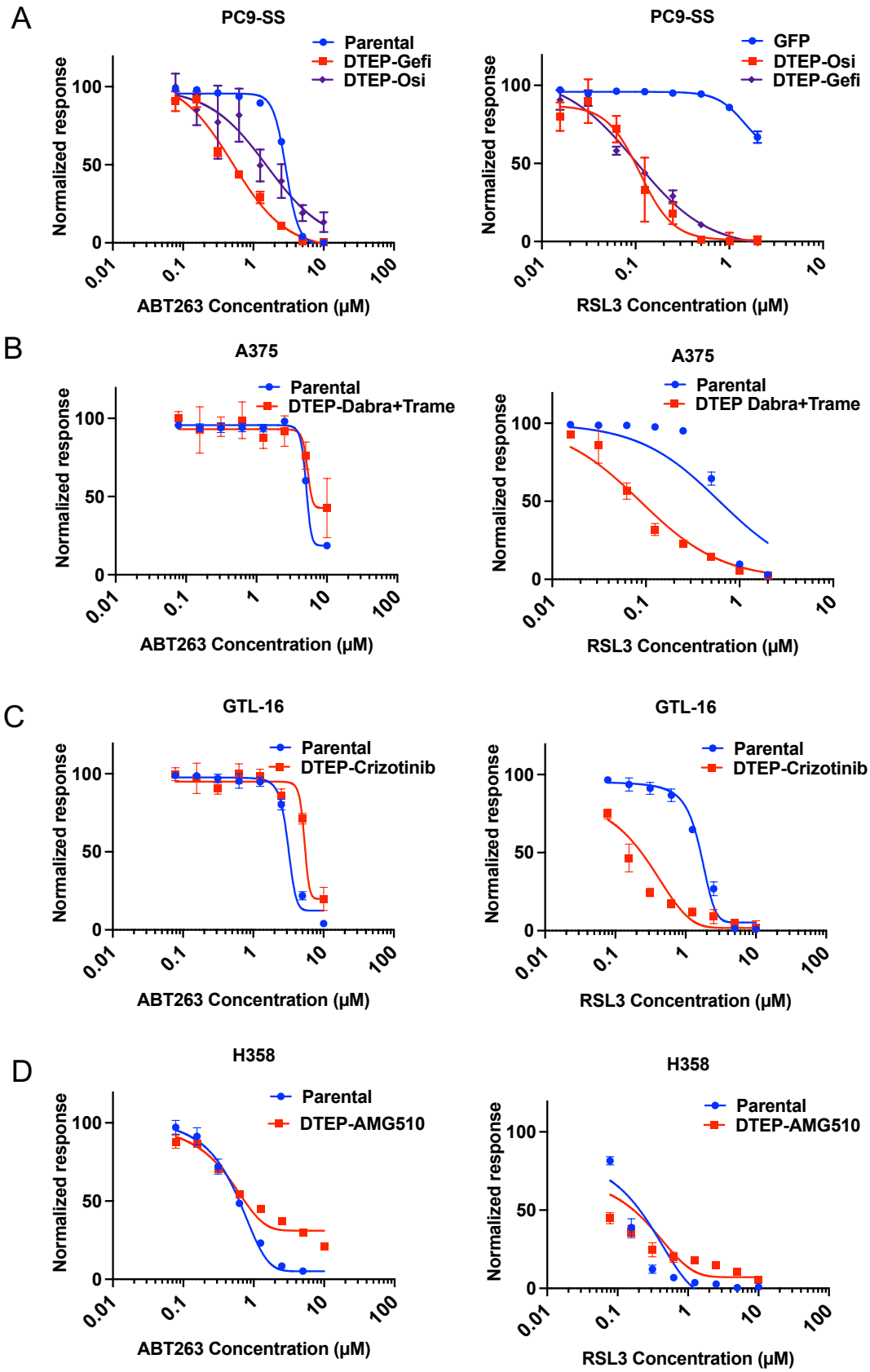

Figure S6. ABT263 selectively eliminated persisters derived from EGFPi induced PC9. No therapeutic window was observed from H358 treated with RSL3. Related to Figures 1 and 2. (A-D) Five-day dose response curve for paired parental and persisters from PC9, A375, GTL-16 and H358 to Bcl family inhibitor ABT263 and GPX4 inhibitor RSL3. Error bars in A-D represent mean ± s.d., n = 3 independent experiments. Statistical significance was calculated by two-tailed Student's t-test.

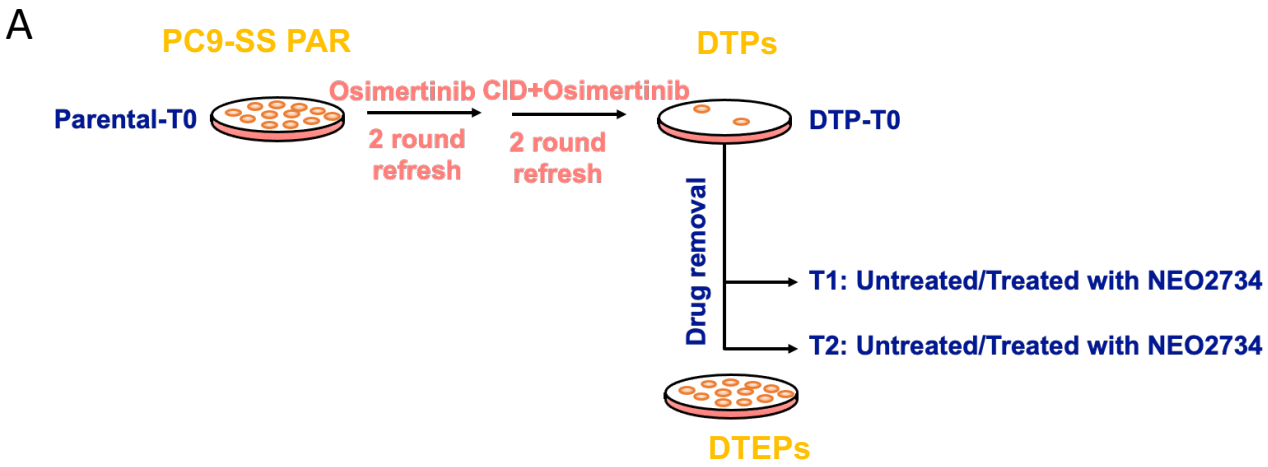

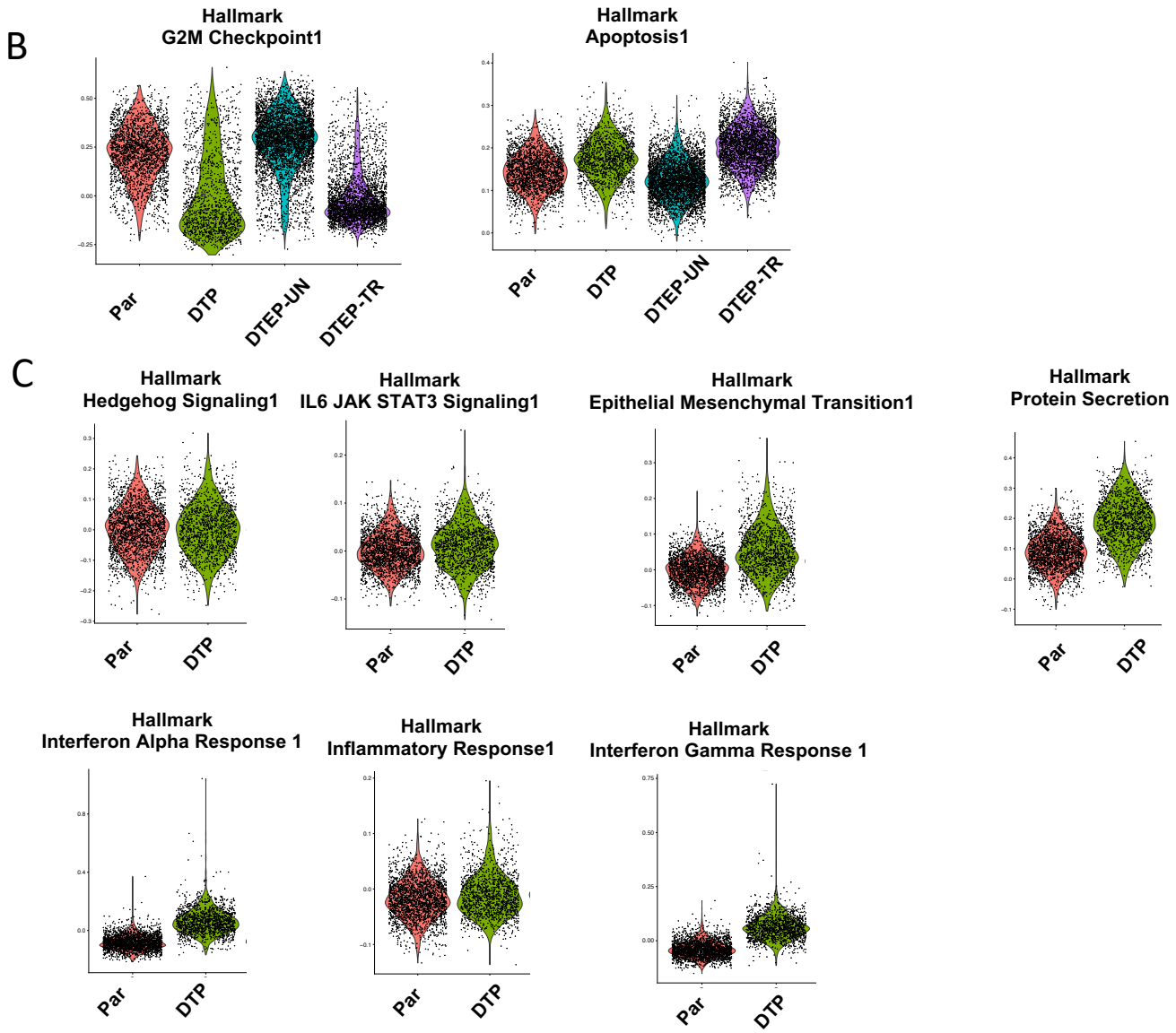

Figure S7. scRNA seq uncovered different gene signature in persisters. Related to Figure 3. (A) Graphic description of scRNA seq sample preparations. (B) Dynamic changes for G2M checkpoint and apoptosis observed in parental, DTP, DTEP and DTEP treated with NEO2734. (C) Representative gene signatures identified in DTPs.

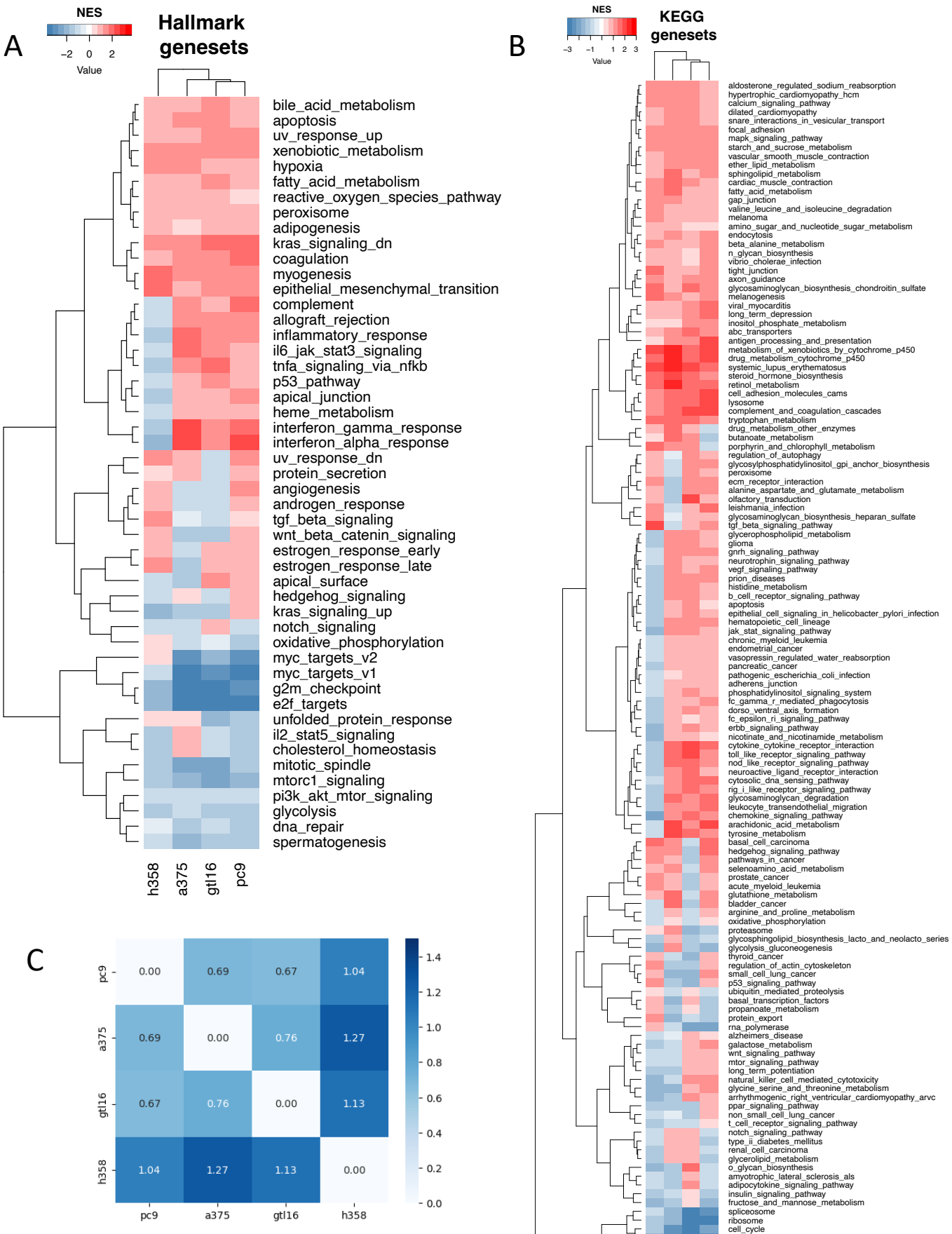

Figure S8. bluk RNA seq based transcriptomic features of DTPs compared with parental controls. Related to Figure 3. (A) GSEA pathway enrichment analysis for DTPs compared with parental controls focusing on Hallmark genesets. (B) GSEA pathway enrichment analysis for DTPs compared with parental controls focusing on KEGG genesets. (C) Heatmap representation for distance among each NES score for paried DTP T0/Parental T0 based on GSEA analysis for both Hallmark and KEGG genesets.

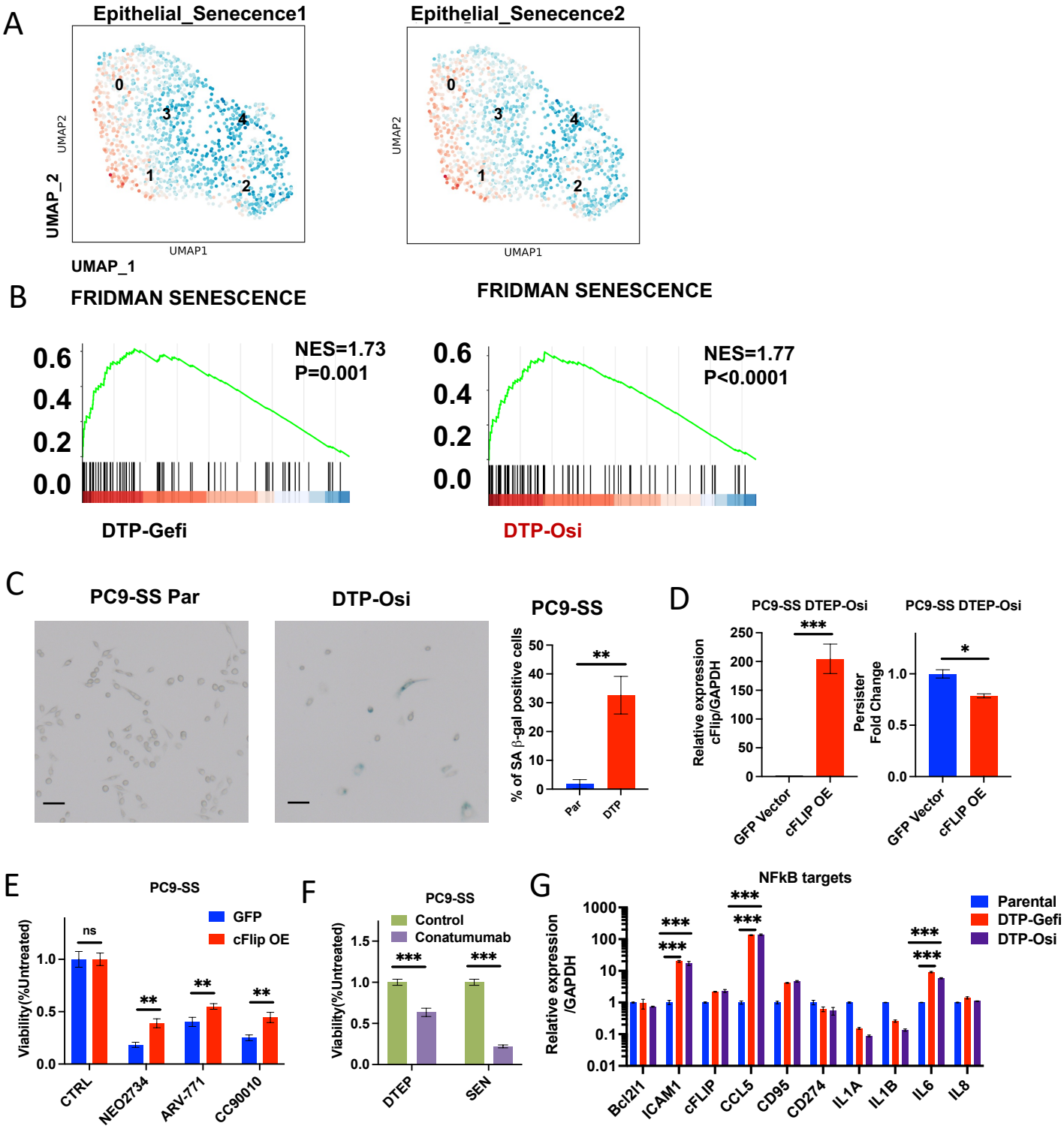

Figure S9. DTPs share some similarities with senescence cells but have different vulnerabilities. Related to Figure 3.
(A) Senesence signature geneset modula score within DTPs. Two epithelial senescence signatures were tested. (B) GSEA analysis for senescence gene signature in DTPs in comparison with parental PC9 cells based on bulk-RNA seq. (C) Senescence-associated β-galactosidase (SA-β-Gal) staining of cells. Left: Representative image; Right: Quantification of left. Black scale bars, 50 µm. (D) cFLIP overexpression efficiency detected by qPCR. Persister cells calculation compared to GFP control. (E) Relative viabilities of DTEPs from GFP and cFLIP^{OE} PC9 treated with three BET inhibitors. NEO2734: 0.08µM; ARV-771: 0.08µM; CC90010: 0.08µM. (F) Relative viabilities of DTEPs and senescent cells from GFP and cFlip^{OE} PC9 treated with Conatumumab. Conatumumab:125ng/ml. (G) Transcriptomic analysis of NF-kB targets in parental PC9, DTP-Gefi and DTP-Osi. Error bars in C-G represent mean ± s.d., n = 3 independent experiments. Statistical significance was calculated by two-tailed Student's t-test (*P ≤ 0.05, ** P ≤ 0.01, *** P ≤ 0.001).

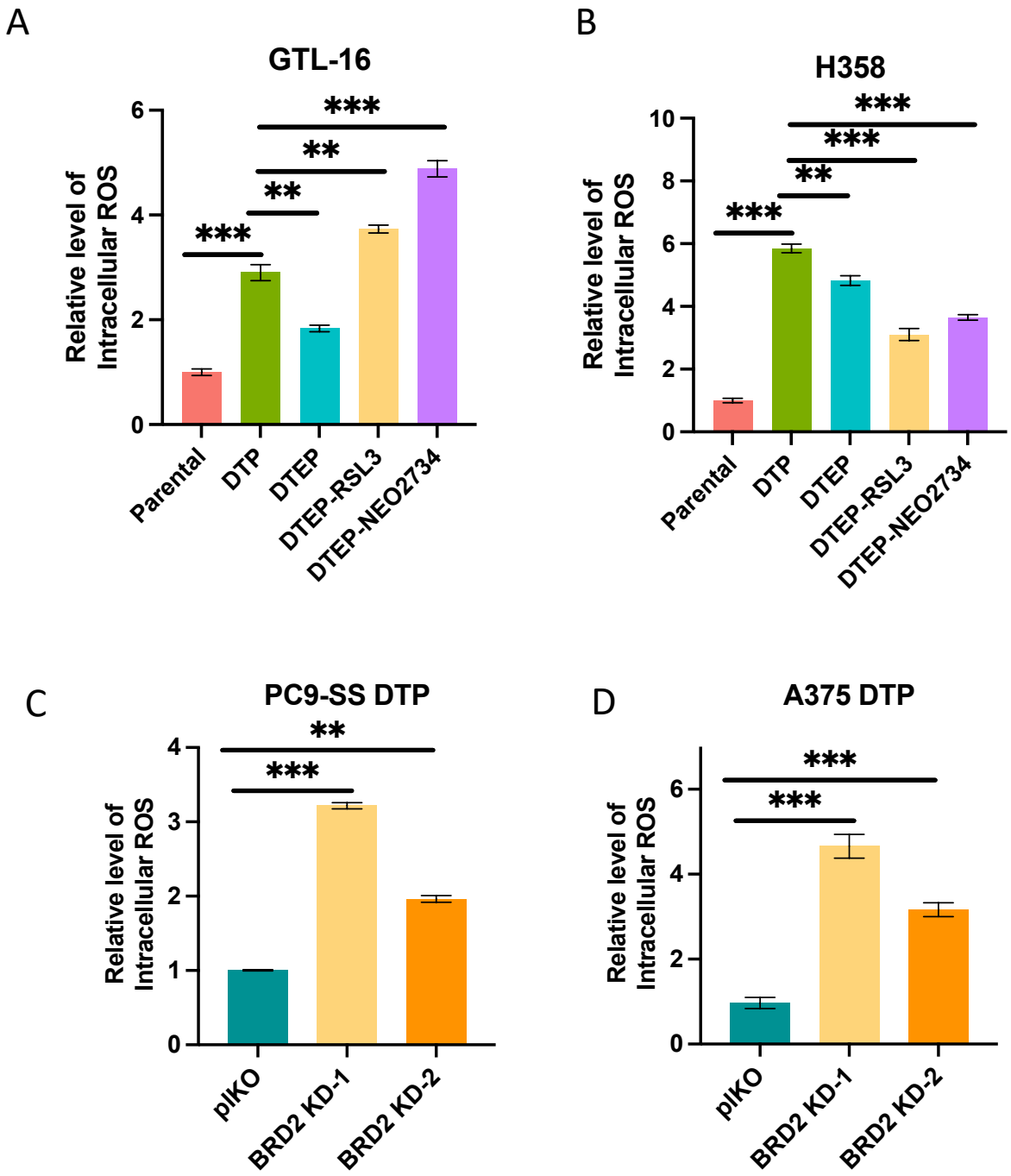

Figure S10. Intracellular ROS staining by flow cytometry in GTL-16 and H358. Related to Figures 4 and 5. (A) Quantifications of intracellular ROS level (mean fluorescent intensity) in parental GTL-16, DTP, DTEP and DTEP challenged with RSL3 and NEO2734. (B) Quantifications of intracellular ROS level (mean fluorescent intensity) in parental H358, DTP, DTEP and DTEP challenged with RSL3 and NEO2734. (C) Quantifications of intracellular ROS level (mean fluorescent intensity) of DTPs from BRD2 knockdown cells compared to plKO cells in PC9-SS. (D) Quantifications of intracellular ROS level (mean fluorescent intensity) of DTPs from BRD2 knockdown cells compared to plKO cells in PC9-SS. Error bars in A-D represent mean ± s.d., n = 3 independent experiments. Statistical significance was calculated by two-tailed Student's t-test (*P ≤ 0.05, ** P ≤ 0.01, *** P ≤ 0.001).

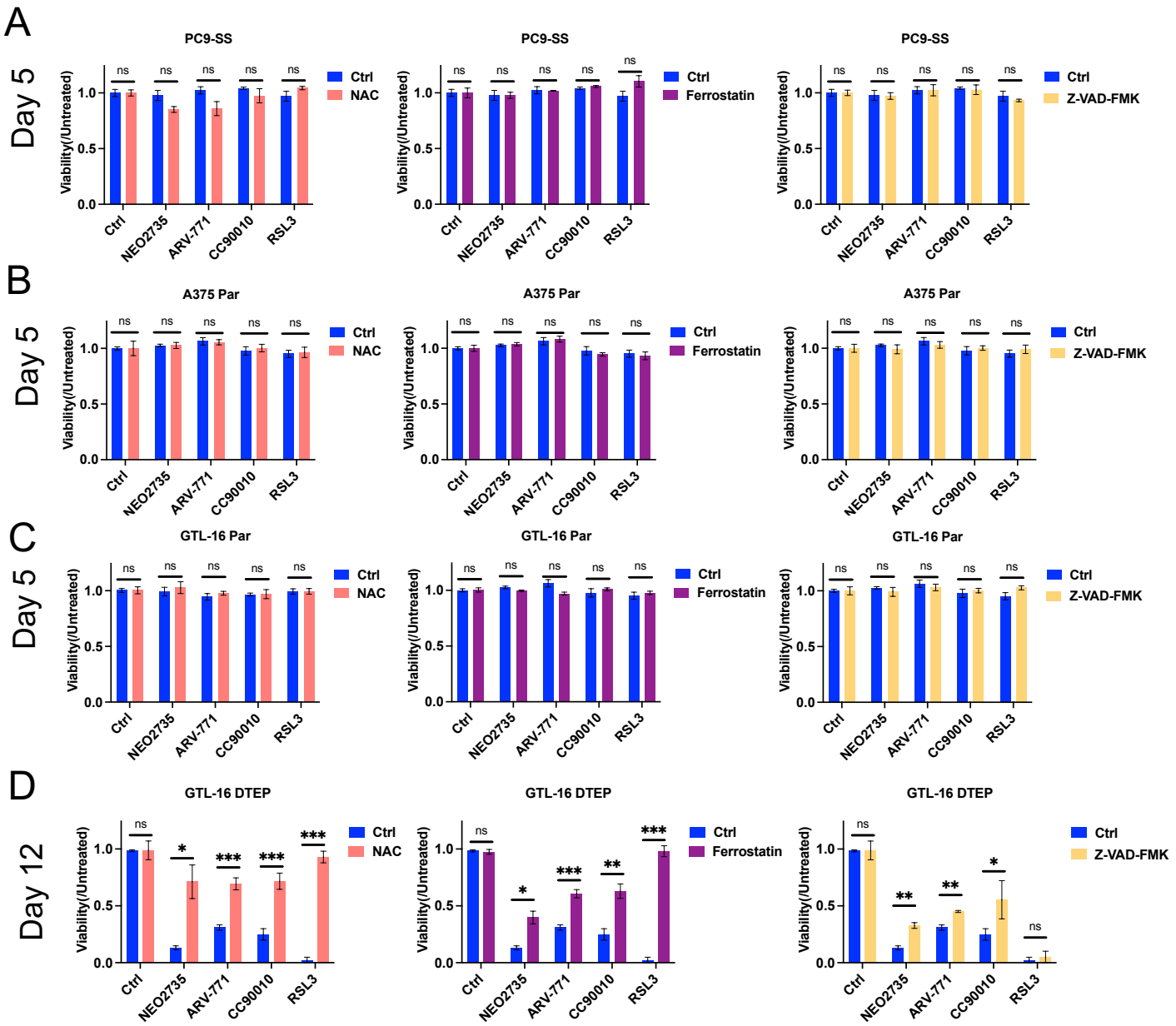

Figure S11. Rescue experiments by NAC, Ferrostatin and Z-VAD-FMK in PC9, A375 and GTL-16 derived DTEPs treated with BET inhibitors. Related to Figures 4 and 5. (A) Relative cell viabilities of parental PC9 treated with NEO2734, ARV-771, CC90010 and RSL3 cultured with or without NAC, Ferrostatin and Z-VAD-FMK. (B) Relative cell viabilities of parental A375 treated with NEO2734, ARV-771, CC90010 and RSL3 cultured with or without NAC, Ferrostatin and Z-VAD-FMK. (C) Relative cell viabilities of parental GTL-16 treated with NEO2734, ARV-771, CC90010 and RSL3 cultured with or without NAC, Ferrostatin and Z-VAD-FMK. (D) Relative cell viabilities of DTEP derived from GTL-16 treated with NEO2734, ARV-771, CC90010 and RSL3 cultured with or without NAC, Ferrostatin and Z-VAD-FMK (NEO2734: 0.25μM; ARV-771: 0.25μM; CC90010: 0.25μM; NAC:2.5mM; Ferrostatin: 2.5μM; Z-VAD-FMK: 10μM). Error bars in A-D represent mean ± s.d., n = 3 independent experiments. Statistical significance was calculated by two-tailed Student's t-test (*P ≤ 0.05, ** P ≤ 0.01, *** P ≤ 0.001).

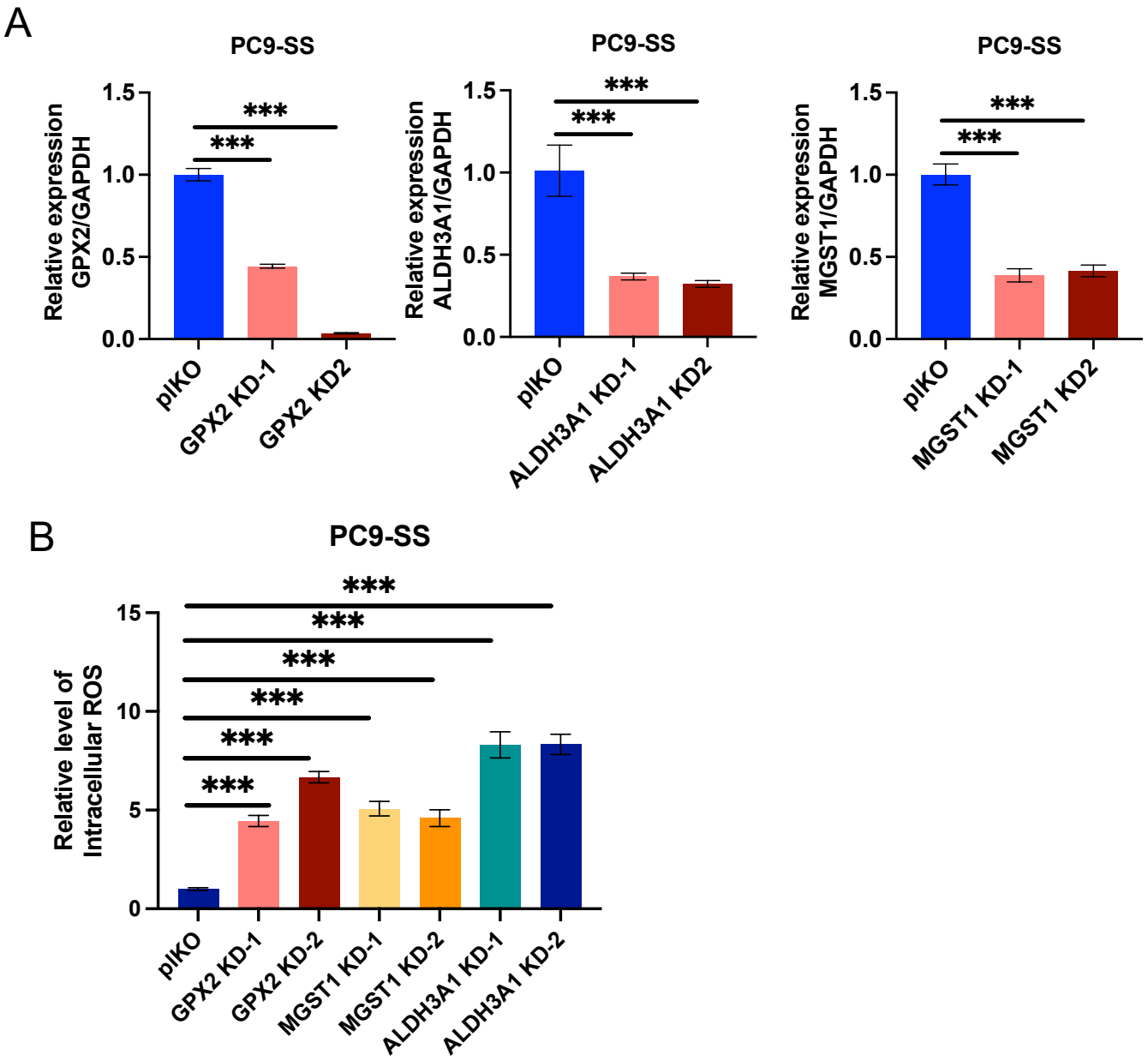

Figure S12. ROS level of DTPs were increased upon knockdown of GPX2, ALDH3A1 and MGST1. Related to Figure 5. (A) Knockdown efficiency of GPX2, MGST1 and ALDH3A1 in PC9-SS by q-PCR. (B) Quantification of intracellular ROS levels (mean fluorescent intensity) of DTPs in plKO, GPX2 KD-1, GPX2-KD2, MGST 1 KD-1, MGST1 KD-2, ALDH3A1 KD-1 and ALDH3A1 KD-2. Error bars in A-B represent mean ± s.d., n = 3 independent experiments. Statistical significance was calculated by two-tailed Student's t-test (*$P \leq 0.05$, ** $P \leq 0.01$, *** $P \leq 0.001$).

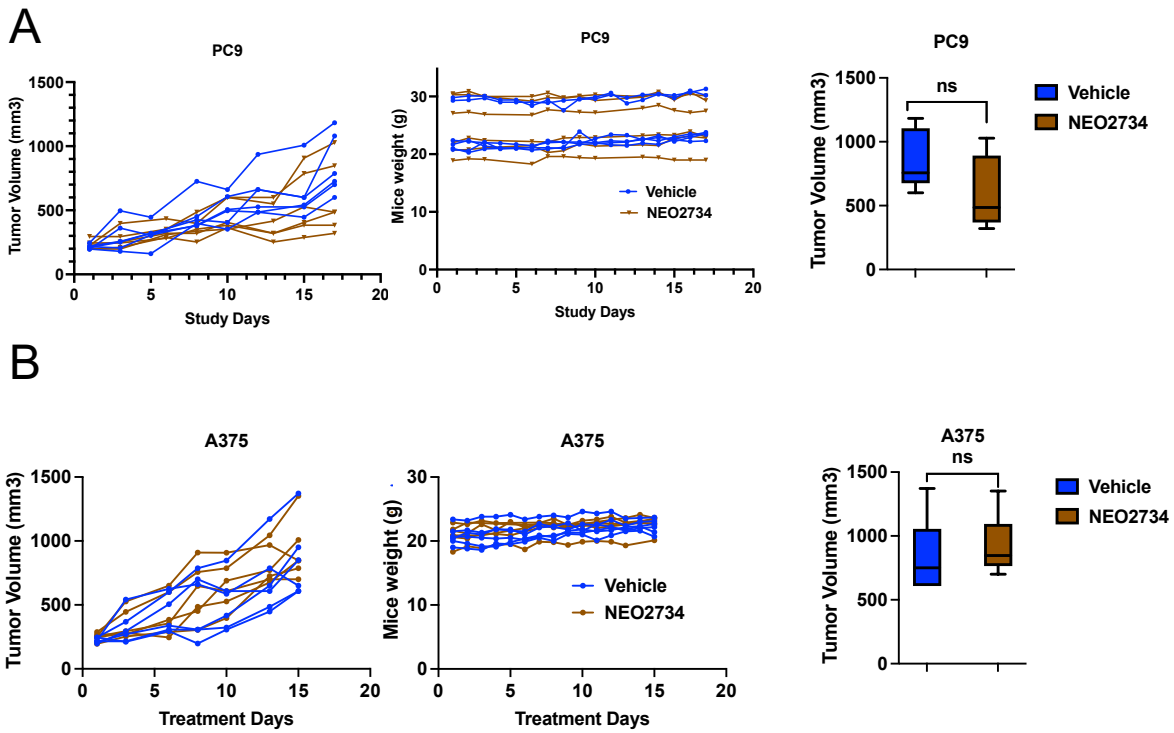

Figure S13. BET inhibitor has minor effect on controlling parental cancer proliferation in vivo. Related to Figure 6. (A) Relative tumor volumes and mice weight for PC9 subcutaneous bearing mice treated with vehicle, NEO2734 (n=6 for each group). (B) Relative tumor volumes and mice weight for A375 subcutaneous bearing mice treated with vehicle, NEO2734 (n=6 for each group). Data are presented as mean ± s.e.m. Two-way analysis of variance (ANOVA) was applied for the in vivo study statistical analysis (*$P \leq 0.05$, ** $P \leq 0.01$, *** $P \leq 0.001$).

Table S2. List of DTP markers and their expression changes in DTEPs upon NEO2734 treatment. Related to Figure 3.

DTP markers	Log2 FC(DTEP TR/UN)	Aver_Differ
ALDH3A1	-4,24792751	1,89131446
CYP1B1	-3,86882918	10,2313782
LYPD6B	-2,37178861	23,6253318
GPX2	-2,15881489	11,0704595
FN1	-1,88328188	5,21058898
ALPP	-1,7684921	8,15688063
S100P	-1,75822321	4,73060596
CCDC80	-1,58230944	6,14430032
SERPINB5	-1,495077	4,03732768
VGLL1	-1,47196457	5,11506143
MGST1	-1,3721061	2,78435996
FXYD3	-1,32192809	16,7187148
IGFBP3	-1,32125574	6,83528438
FBP1	-1,30142978	12,4883401
ARHGDIB	-1,17023692	11,0335559
RBM47	-1,12890212	24,5836547
TPD52L1	-1,12657188	5,84317502
CXXC5	-0,94981424	7,57707816
TNS3	-0,91737317	18,3930842
RPL37	-0,87334095	0,74569086
CAMK2N1	-0,78580473	17,7801061
GNAQ	-0,78300339	12,346179
PCDH7	-0,77356121	7,18389647
PLS3	-0,71814063	7,81059494
TNFAIP2	-0,68492254	8,1285217
MAL	-0,67855938	18,0648175
PRXL2A	-0,67719781	4,61986633
TMEM45B	-0,60847331	6,9806803
MARCKS	-0,57872439	9,97916452
LIMCH1	-0,53476096	11,1598565
CDKN2A	-0,49811924	15,1279592
LCN2	-0,48433738	2,93410644
CAMK2G	-0,46497628	16,2216722
CTSD	-0,4358519	0,19504952
CTSH	-0,38861432	5,82573071
RPS12	-0,38145905	0,36583016
SKIL	-0,35361539	10,7074503
TMEM139	-0,2833068	13,8833255
ATXN10	-0,27397375	6,04671629
PLAAT3	-0,22948185	10,6750645
MUC20	-0,15600502	6,74053935

DAPK1	-0,10568917	14,3203738
PSCA	-0,03783207	6,56881003
PDLIM1	0,09297777	17,0282715
SH3YL1	0,13521414	10,1606966
EZR	0,18473501	4,89626196
FBLN1	0,22287053	8,47485305
ANXA4	0,23157893	8,29378063
PDGFD	0,24259765	11,3406825
TSTD1	0,24392558	12,0886066
MT-CO3	0,25691449	6,64883653
PCSK5	0,47978787	5,54494723
SEMA5A	0,48122412	9,11149452
GSTK1	0,5687882	21,7718524
JDP2	0,56889181	14,031336
SPINT2	0,57939187	1,48930862
CD9	0,62002364	4,84567969
MAN1A1	0,74029976	18,6314181
QPRT	0,80279664	15,2491275
ASAH1	0,85656868	9,81037049
KRT7	0,86098473	2,181738
LGALS3	0,98274867	20,0718399
KRT19	1,12169516	1,4909795
GABARAP	1,14438991	4,29122683
MYH14	1,16021737	24,5180585
TRAPPC6A	1,17632277	8,29220981
CD24	1,24603979	15,6185246
TACSTD2	1,258863	3,34741067
TMC4	1,43609911	7,5342684

Table S3. List of primers. Related to Figures 1&5 and STAR Methods.

qPCR primers

Name	**Sequence**
ALDH3A1-F	TGGAACGCCTACTATGAGGAG
ALDH3A1-R	GGGCTTGAGGACCACTGAG
MGST1-F	GCCCACCTGAATGACCTTGA
MGST1-R	GTCTGAAGTGCAGGATGGCT
GPX2-F	GACTTCACCCAGCTCAACGA
GPX2-R	CCCCAGGACGGACATACTTG
GAPDH-F	GAAGGTGAAGGTCGGAGTC
GAPDH-R	GAAGATGGTGATGGGATTTC
cFlip-F	GTTCAAGGAGCAGGGACAAG
cFlip-R	TCCCATTTATGGAGCCTGAAG
BCL2L1-F	GTAAACTGGGGTCGCATTGT
BCL2L1-R	TGGATCCAAGGCTCTAGGTG
ICAM1-F	ATGCCCAGACATCTGTGTCC
ICAM1-R	GGGGTCTCTATGCCCAACAA
CCL5-F	CCAGCAGTCGTCTTTGTCAC
CCL5-R	CTCTGGGTTGGCACACACTT
CD95-F	TCTGGTTCTTACGTCTGTTGC
CD95-R	CTGTGCAGTCCCTAGCTTTCC
CD274-F	TATGGTGGTGCCGACTACAA
CD274-R	TGGCTCCCAGAATTACCAAG
IL-1A-F	AGATGCCTGAGATACCCAAAACC
IL-1A-R	CCAAGCACACCCAGTAGTCT
IL-1B-F	AAGCCCTTGCTGTAGTGGTG
IL-1B-R	GAAGCTGATGGCCCTAAACA
IL-6-F	ACTCACCTCTTCAGAACGAATTG
IL-6-R	CCATCTTTGGAAGGTTCAGGTTG
IL-8-F	TCCTGATTTCTGCAGCTCTGT
IL-8-R	AAATTTGGGGTGGAAAGGTT
BRD2-F	GAGGTGTCCAATCCCAAAAAGC
BRD2-R	ATGCGAACTGATGTTTCCACA
BRD3-F	CTGAAACCCACCACTTTGCG
BRD3-R	GCTCCTCTTTCGACTTGGCT
BRD4-F	ACCTCCAACCCTAACAAGCC
BRD4-R	TTTCCATAGTGTCTTGAGCACC

shRNA sequence:

shBRD2#1	CCGGGCCCTCTTTACGTGATTCAAACTCGAGTTTGAATCACGTAAAGAGGGCTTTTT
shBRD2#1	CCGGCCCTGCCTACAGGTTATGATTCTCGAGAATCATAACCTGTAGGCAGGGTTTTT
shBRD3#1	CCGGCCCAAGAGGAAGTTGAATTATCTCGAGATAATTCAACTTCCTCTTGGGTTTTT
shBRD3#2	CCGGGCTGATGTTCTCGAATTGCTACTCGAGTAGCAATTCGAGAACATCAGCTTTTT
shBRD4#1	CCGGCCTGGAGATGACATAGTCTTACTCGAGTAAGACTATGTCATCTCCAGGTTTTTG
shBRD4#2	CCGGCCCTTTGCTGTGACACTTCTTCTCGAGAAGAAGTGTCACAGCAAAGGGTTTTT
shGPX2#1	CCGGCCTTGCAACCAATTTGGACATCTCGAGATGTCCAAATTGGTTGCAAGGTTTTTG
shGPX2#2	CCGGCCGATCCCAAGCTCATCATTTCTCGAGAAATGATGAGCTTGGGATCGGTTTTTG
shALDH3A1#1	CCGGGCTAAGAAATCCCGGGACTATCTCGAGATAGTCCCGGGATTTCTTAGCTTTTT
shALDH3A1#2	CCGGCCTGCACAAGAATGAATGGAACTCGAGTTCCATTCATTCTTGTGCAGGTTTTT
shMGST1#1	CCGGGCCAATATCCTGTATTCTTGTCTCGAGACAAGAATACAGGATATTGGCTTTTTTG
shMGST1#2	CCGGCATACAACTCAGCATCCAGTTCTCGAGAACTGGATGCTGAGTTGTATGTTTTTG